Applied Geochemistry 92 (2018) 121–139

Contents lists available at ScienceDirect

Applied Geochemistry

journal homepage: www.elsevier.com/locate/apgeochem

Effects of reclaimed water discharge in the Maneadero coastal aquifer, Baja California, Mexico

Christian Gilabert-Alarcón[a,d], Luis W. Daesslé[a,*], Saúl O. Salgado-Méndez[a], Marco A. Pérez-Flores[b], Kay Knöller[c], Thomas G. Kretzschmar[b], Christine Stumpp[d,e]

[a] Universidad Autónoma de Baja California, Instituto de Investigaciones Oceanológicas, Doctorado en Medio Ambiente y Desarrollo, Carretera Transpeninsular Ensenada-Tijuana, No 3917, Fraccionamiento Playitas, C.P. 22860, Ensenada, Baja California, Mexico
[b] División de Ciencias de la Tierra, Centro de Investigación Científica y de Educación Superior de Ensenada CICESE, Carretera Ensenada, Tijuana, No 3918, Zona Playitas, C.P. 22860, Ensenada, B.C, Mexico
[c] Department of Catchment Hydrology, UFZ-Helmholtz Centre for Environmental Research, Theodor-Lieser-Str. 4, D-06120, Halle, Germany
[d] Institute of Groundwater Ecology, Helmholtz Zentrum München-German Research Center for Environmental Health, Ingolstädter Landstr. 1, D-85764, Neuherberg, Germany
[e] Institute of Hydraulics and Rural Water Management, University of Natural Resources and Life Sciences, Muthgasse 18, 1190, Vienna, Austria

ARTICLE INFO

Handling Editor: Prof. M. Kersten

Keywords:
Coastal aquifers
Salinization
Reclaimed water
Groundwater quality
Hydrochemical processes

ABSTRACT

Since 2014, reclaimed water has been used for agricultural irrigation and it has been discharged on a riverbed of the Maneadero aquifer, Baja California, Mexico. To determine the effects of reclaimed water on groundwater quality, samples of reclaimed water and groundwater were collected spatiotemporal and analyzed using stable isotope ($\delta^{18}O_{H2O}$, $\delta^{2}H_{H2O}$, $\delta^{18}O_{NO3}$ and $\delta^{15}N_{NO3}$) and geochemical signatures, jointly with multivariate statistical methods and a 2D resistivity tomography. Reverse ion exchange and mineralization are the main processes influencing the groundwater composition. The Cl/Br ratios identified seawater intrusion and solid waste, wastewater and animal waste as the main sources responsible for these processes, overlapping with the ratios of reclaimed water. Nitrates are pervasive throughout the aquifer and $\delta^{18}O_{NO3}$ and $\delta^{15}N_{NO3}$ attributed wastewater and animal waste as the major nitrates inputs. Multivariate statistics were able to separate seawater and human-derived processes. The $\delta^{18}O_{H2O}$ and $\delta^{2}H_{H2O}$showed the effect of mixing with *d*-excess of 5–6‰, indicating recharge other than precipitation. A mixing model using Cl^{-} and $\delta^{18}O_{H2O}$ and principal components revealed the mixing proportion of seawater; whilst the over- and under-estimates of reclaimed water contribution are indicative of missing end-members. The Na-Cl-Br-B systematics, however, suggest that reclaimed water result in cation-exchange and adsorption reactions and once the adsorbed sites become saturated with respect of Na^{+}, $Br^{-}$and B^{-}can be reflected in the groundwater composition. Additionally, resistivities indicate that reclaimed water interacts between the fresh and brackish groundwater. Monitoring the efficiency of the vadose zone to retain contaminants and distinguish them from reclaimed water is essential for evaluating groundwater quality.

1. Introduction

Water is a scarce resource in arid regions and the great demand of water from aquifers threatens water supply, particularly in coastal areas. This over-abstraction leads to depletion of groundwater and to groundwater salinization as seawater intrusion flows inland, resulting in adverse economic and environmental impacts (Goebel et al., 2017). Additionally, the high levels of salt in irrigation and the use of fertilizers can also contribute to groundwater salinization (Foued et al., 2011). Municipal reclaimed water (RW) has successfully been used worldwide for aquifer recharge and crop irrigation in order to overcome groundwater quality deterioration and to increase water availability (Murray, 2008; Voudouris, 2011 and references therein). Major challenges associated with these practices include health risks and environment pollution due to the transport of contaminants and pathogens in RW (Asano and Cotruvo, 2004; Toze et al., 2004). To obtain an adequate treatment of the effluent and attenuate groundwater contamination, the hydrochemical processes, including the long-term (geological) and recent (anthropogenic) sources influencing groundwater composition with respect to space and time need to be understood. Understanding the processes and factors that control water quality in the aquifers has important implications for water resource

* Corresponding author.
E-mail address: walter@uabc.edu.mx (L.W. Daesslé).

https://doi.org/10.1016/j.apgeochem.2018.03.006
Received 24 January 2018; Received in revised form 4 March 2018; Accepted 5 March 2018
Available online 08 March 2018
0883-2927/

(a)

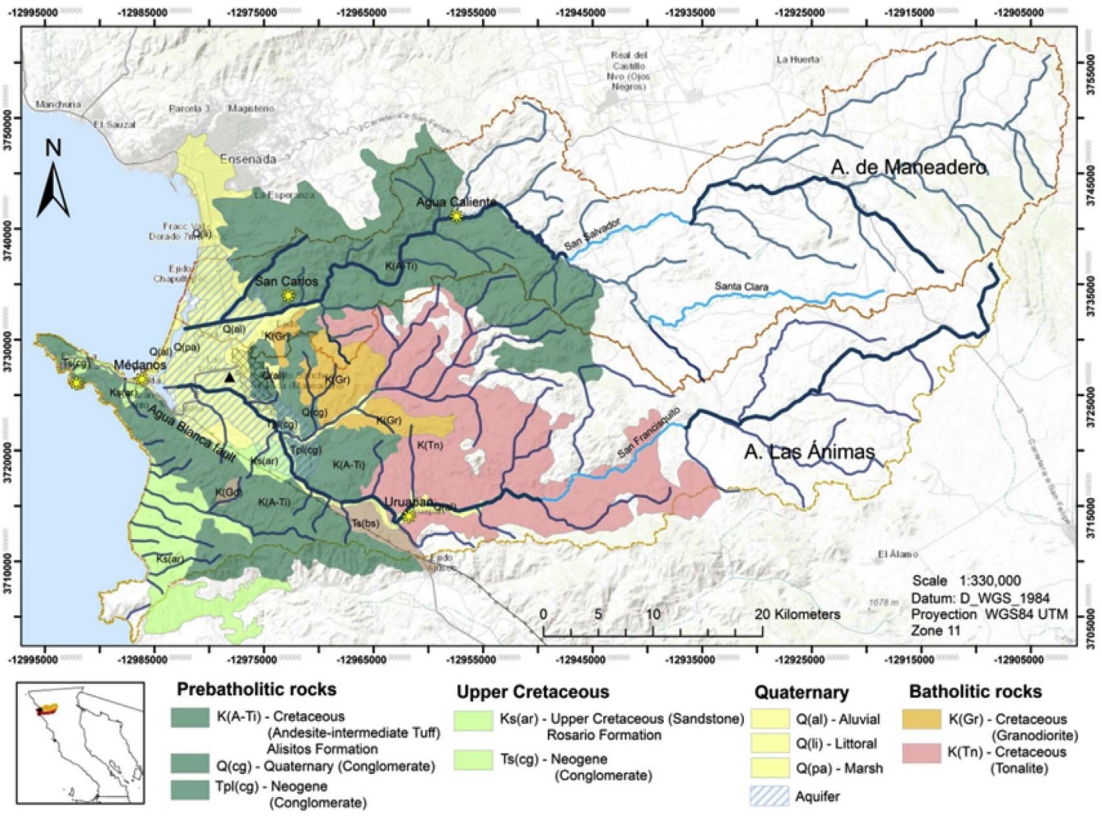

(b)

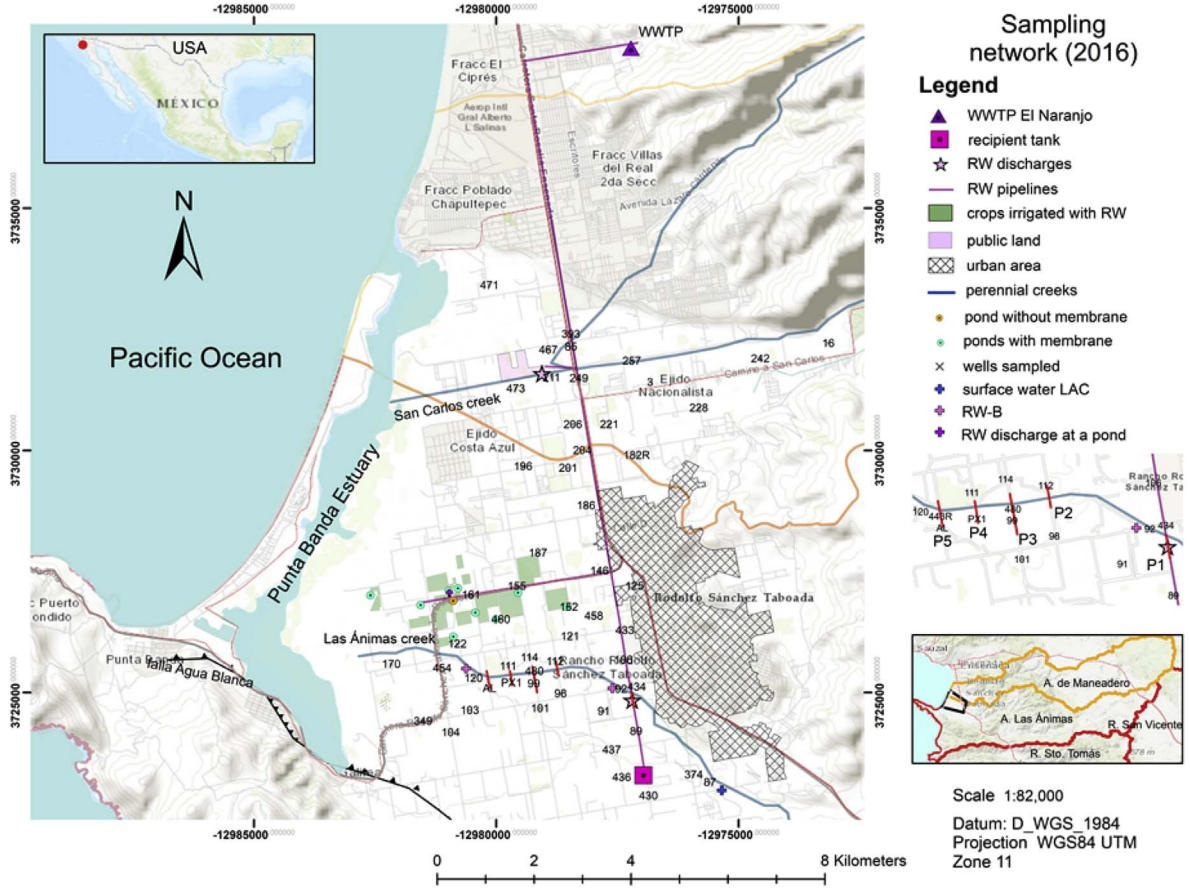

(caption on next page)

Fig. 1. (a) Lithological features and hydrological basin of the Maneadero valley. The *yellow symbols* indicate the location of the hot springs and the *triangle symbol* the location of Maneadero urban area; (b) Location of the sampled wells and the RW discharge sites, and of the five geophysical sections across Las Animas creek (profiles P1-P5). (For interpretation of the references to color in this figure legend, the reader is referred to the Web version of this article.)

management (Bouchaou et al., 2008).

Geochemical indicators are used to assess the hydrodynamics of the aquifer such as groundwater flow, recharge rate, chemical weathering of the various rock types and mixing between different sources other than water-rock interaction (De Montety et al., 2008; Madioune et al., 2014; Okiongbo and Douglas, 2015; Vengosh et al., 2002). In the context of use of RW for artificial aquifer recharge, several studies have evaluated the quality of the effluent after the recovery (De Bustamante et al., 2010; Kanarek and Michail, 1996; Missimer et al., 2012; Vandenbohede et al., 2009), as well as recharge associated with the use of RW for irrigation and leakages from water supplies (Chen et al., 2006; Vengosh et al., 1998; Wang et al., 2014). The use of potential markers has also been investigated to trace the mixing and travel times of RW using major and minor ions. Massman et al. (2004) estimated the proportions of treated wastewater from K^+, EDTA and B^-, and Bekele et al. (2011) found the mixing with RW on the basis of K^+ and Cl^- concentrations. Kloppman et al. (2009) compared an artificial salt tracer (KBr) with boron and lithium isotopes for tracing treated wastewater. Lithium isotopes proved to be valuable tracers, but were more affected by sorption processes when compared to Br^-. Bekele et al. (2014) compared Br^-, Cl^- and water temperature as tracers and provided consistent results with respect to estimating the residence time of reclaimed water. The authors emphasized that results relied on data from observation wells that intercepted flow paths and none from abstraction wells due to significant dilution from pumping. Whilst tracers yielded similar residence times, the analysis of Cl^- and Br^- tracers revealed discrepancies, suggesting that a revised conceptual model of the aquifer (i.e. transport directions) was required. Donohue et al. (2015) applied geoelectrical measurements together with hydrogeological data to characterize recharge-induced changes on groundwater, demonstrating that geological settings need to be considered for correct interpretations. Although several tracers have demonstrated to be effective tools to trace the effluent recharge, these tracers are not straight forward because both the input (effluent) and the background (groundwater receptor) concentrations are highly variable both spatially and temporally (Rueedi et al., 2009); and therefore, tracer results must be interpreted with care, particularly in areas with multi-modal flows (De Vries and Simmers, 2002).

Incidental recharge of groundwater from RW used for agricultural irrigation and/or discharges to rivers unrelated to an artificial recharge project usually occurs in developing countries. In most cases, the physical, chemical and biological reactions and the impacts that take place in the aquifer are poorly quantified (Fosters et al., 2003). One example of this in arid water systems in Mexico is the Colorado River delta (Orozco-Durán et al., 2015; Daesslé et al., 2016, 2017). Another example is the use of RW for agricultural irrigation and discharge of the effluent in the coastal aquifer of Maneadero (Baja California, Mexico). Over the past five decades, the low rainfall and over-abstraction of this aquifer has resulted in seawater intrusion (CONAGUA, 1999; Daesslé et al., 2014). In consequence, salinity has caused severe deterioration of groundwater quality for agriculture and domestic water supply, resulting in several wells being abandoned in the last 5 years. To reduce the stress on water supplies and prevent seawater intrusion, in 2014, a project initiated to irrigate 100 ha of flowers with RW and to discharge the effluent into the creeks recharging the aquifer. However, the use and the discharge of RW in the valley are disputed because there is not enough knowledge about the RW and its impacts on groundwater quality and public health that may result from aquifer recharge.

The aim of the present study is to assess the processes that have affected the groundwater quality during the first three years of aquifer recharge by using hydrochemical tracers such as major ion composition and stable isotopes of water ($\delta^{18}O_{H2O}$ and $\delta^{2}H_{H2O}$) and of nitrates ($\delta^{18}O_{NO3}$ and $\delta^{15}N_{NO3}$), jointly with multivariate statistical methods and electrical 2D resistivity tomography. This study is intended to be the scientific baseline for aquifer recharge projects in the region and be adapted into similar sites where coastal aquifers are depleted by over-abstraction.

2. Methods

2.1. Study area

Maneadero Valley is located 15 km south of Ensenada, Baja California, at 31°41′N and 116°30′W (Fig. 1) and it is situated within the "Sierra-Juárez-San Pedro Mártir" physiographic province (Álvarez, 1949). The geological setting and hydrogeology have been described in detail by Daesslé et al. (2014). The catchment area comprises two perennial creeks which drain mainly during the winter rain season: San Carlos creek at the Arroyo de Maneadero watershed and Las Ánimas-San Francisquito, Las Ánimas creek at the Arroyo Las Ánimas watershed (Fig. 1a and b). Both creeks drain 1879 km^2 and the studied aquifer has an extension of 130 km^2. The annual runoff of the San Carlos creek is in average 10.34 Mm^3 and of the Las Ánimas 22.96 Mm^3 (Venegas, 2007). Mixed hydrothermal systems surround the coastal aquifer of Maneadero (Vidal-Lorandi and Vidal-Lorandi, 2003): to the NE the hot springs of the San Carlos and Agua Caliente emerge from the upper section of the San Carlos creek, to the SE the Uruapan hot spring lies within the Agua Blanca Fault and it is located in the upper part of the Las Ánimas creek and two hot springs (Punta Banda and Médanos de Punta Banda) are located along the northern side of the Punta Banda sector (Fig. 1a).

The climate is semi-arid and the mean annual temperature and precipitation are 16.6 °C and 253 mm respectively, with rainy season in winter (CONAGUA, 1999). Agriculture constitutes the traditional economic activity of the area and the main crops have been alfalfa, olive, corn and some vegetables, with an increasing production of high quality greenhouse horticulture for export, with a total crop area of 5300 ha.

Groundwater is extracted from ca. 350 active wells of which seven supply the cities of Ensenada-South and Maneadero. The average depth of wells is between 25 and 50 m (Daesslé et al., 2014). According to official data, the aquifer over-abstraction is estimated at 17 Mm^3 (DOF, 2015). In order to use RW as a water source, in 2008, a 20 km pipeline was built to connect the wastewater treatment plant (WWTP) of El Naranjo with a holding tank of 2000 m^3 (Fig. 1b). In 2014, a 4 km long pipeline was installed connecting the WWTP main pipe from El Naranjo to irrigate abandoned agricultural land near the coast, namely for floriculture (such as sunflowers) and fodder (alfalfa). In addition, two pipelines were built to discharge the effluent in a public land nearby the San Carlos creek and ca. 14,500 m^3/d into the Las Ánimas creek.

The effluent from El Naranjo is categorized as "disinfected secondary 2.2" by the California Code of Regulation of the State of California (2000), meaning that the median concentration of total coliform bacteria does not exceed a most probable number (MPN) of 2.2 per 100 mL for 7 days. The WWTP of El Naranjo receives urban wastewater for which the original water source are six wells nearby the San Carlos creek within the same Maneadero aquifer; thus, a similar chemical composition to that of the local groundwater is expected for the effluent.

The variability of water quality in the aquifer of Maneadero due to seawater intrusion and nitrate pollution was first studied by Daesslé et al. (2005, 2009) who described the constant progression of seawater intrusion in the central and southern coastal sections and characterized

the groundwater as an intermediate Na-Cl to Ca-Cl water type. Based on geochemical characteristics and well locations, Daesslé et al. (2014) identified four water quality zones, including one in which nitrates are significantly enriched (with concentrations > 40 mg/L NO_3^--N).

2.2. Sampling

Fifty-seven groundwater samples were taken once during April 2016 from wells throughout the aquifer and repeatedly during rain and drought seasons (November 2015, April 2016, March 2017 and August 2017) from 18 to 20 wells where RW discharges take place (Fig. 1b). RW was sampled from the discharge points at the San Carlos and Las Ánimas creeks, at an irrigation pond and along the RW-flooded Las Ánimas creek (RW-B). The wells were running at the moment of sampling or allowed to run for 10 min. Each of the water samples was filtered with 0.45 μm Millipore® and collected in decontaminated polyethylene bottles. Samples were acidified with 0.1 N trace metal grade HNO_3^- for cation analysis and stored at 4 °C. Those for nutrient analyses were frozen.

2.3. Analytical procedures

The pH, temperature and electrical conductivity (EC) were measured *in situ* using an YSI6600 probe. Total dissolved solids (TDS) were calculated automatically using a 0.65 conversion factor from conductivity and temperature. Cations (Na^+, K^+, Mg^{2+} and Ca^{2+}) were determined using an Agilent 8800 ICP-MS instrument (Agilent Technologies, Japan). Hardness was calculated according to Todd (1980). Anions (Cl^-, SO_4^{2-}, PO_4^{3-}P and Br^-) were analyzed by Ion chromatography (ICS 5000, Thermo Scientific) with a Dionex Anion Self-Regenerating suppressor (Dionex ARS-400 4 mm). Acid titration with 0.5 N HCl was used to determine the concentration of bicarbonate (HCO_3^-) and carbonate ion (CO_3^{2-}). Nitrate (expressed as NO_3^--N) was measured with a Skalar San Plus flow analyzer and boron (B^-) was analyzed by Coupled-Plasma Optical-Emission-Spectrometer (ICP-OES). For cations and anions, the relative standard deviation of the replicate samples was less than 3%. The ion-balance error was calculated using the Freeze and Cherry (1979) definition. Calculated charge balance errors were found to be less than ± 5%. In addition, the analytical check described in Hounslow (1995) was considered for the testing error.

Water Stable isotopes ($\delta^{18}O_{H2O}$ and δ^2H_{H2O}) were determined using a water isotope analyzer (2130, Picarro Inc. Santa Clara, USA), with an accuracy of ± 0.2‰ for δ^2H and ± 0.04‰ for $\delta^{18}O$. The nitrogen and oxygen isotope analyses of nitrate were conducted on a GasBenchII/delta V plus combination (Thermo) using the denitrifier method for a simultaneous determination of $\delta^{15}N$ and $\delta^{18}O$ in the measuring gas N_2O, produced by a controlled reduction of sample nitrate (Casciotti et al., 2002; Sigman et al., 2001). The standard deviation of the measurement were ± 1.6‰ for $\delta^{18}O$ and ± 0.4‰ for $\delta^{15}N$. All the stable isotopic compositions are reported in per mil (‰) relative to their corresponding international standards (V-SMOW for $\delta^{18}O$ and δ^2H, AIR for $\delta^{15}N$).

2.4. Hydrochemistry

Chemical facies and dominant chemical processes were examined by various graphical methods such as Piper (1944) and Stiff (1951) using the computer program Diagrammes Version 6.5 (Laboratoire d`Hydrogéologie d'Avignon, 2017). The hydrochemical characterization was complemented estimating the two chloro-alkaline indices (CAI-1 and CAI-2) according to Custodio and Llamas (1996). In order to study the chemical equilibrium existing in groundwater from the study area, mineral saturation indices (SI) were calculated with respect to five minerals (anhydrite, calcite, dolomite, gypsum and halite) using the code PHREEQC (Pakhurst and Appelo, 1999) from the computer program Diagrammes Version 6.5 (Laboratoire d`Hydrogéologie d'Avignon, 2017).

The theoretical fraction of seawater contribution (f_{SW}) in mixed freshwater was estimated from a mass balance equation using Cl^- according to Appelo and Postma (2005). The aquifer system receives a component of freshwater from two creeks; hence, two samples: well 242 and the surface water of the Las Animas creek, LAC (collected during a rainy season) were considered as end-members. The f_{SW} was then used to determine the ionic deltas (Δ) of Na^+, Ca^{2+} and Mg^{2+} from the mixed composition during the fresh-saline mixing. A three end-member mixing analysis (EMMA) was employed to trace the mixing proportion of RW. For this purpose, the concentrations (C) of the end-member for seawater (C_{SW}), RW (C_{RW}) and the two freshwater (C_{FW}) were used to calculate fractions of water sources using the most conservative pair of traces (t1 and t2)in each sample (C_s) as follows:

$$C_s^{t1} = C_{SW}^{t1} fSW + C_{RW}^{t1} fRW + C_{FW}^{t1} fFW \quad (1)$$

$$C_s^{t2} = C_{SW}^{t2} fSW + C_{RW}^{t2} fRW + C_{FW}^{t2} fFW \quad (2)$$

$$f_{SW} + f_{RW} + f_{FW} = 1 \quad (3)$$

A three-EMMA was then applied using principal component analysis (PCA) as described by Barthold et al. (2011) and Christophersen and Hooper (1992) following the same set of equations in Eqs. (1)–(3).

Groundwater suitability for domestic purposes is weighed based on the synthetic pollution index (SPI) (Gautam et al., 2015):

$$K = \frac{1}{\sum_{i=1}^{n} 1/S_i} \quad (4)$$

$$W_i = K/S_i \quad (5)$$

$$I = \sum_{i=1}^{n} \frac{C_i}{S_i} * W_i \quad (6)$$

where I stands for synthetic pollution index; C_i is the measured concentration of the parameter; S_i is the World Health Organization standard values for the parameter (WHO, 2011); W_i is the weight coefficient and K is constant of proportionality.

Static levels for 2016 by the Comité Técnico de Aguas Subterráneas (COTAS) of Maneadero were used to model the groundwater table and flow direction. The Arc map version 10.2 (ERSI, 2017) was used for mapping the regional distributions of SPI values, TDS concentrations and groundwater level with a GIS-based geostatistical model with the Kriging spatial interpolation technique. The geostatistical interpolation was adopted following the steps described by Machiwal and Madan (2015). Details of the geostatistical models and their theory can be found in Isaaks and Srivastava (1989) and Kitanidias (1997). The geostatistical model for groundwater level was used to model the flow direction by ArcHydro Groundwater (AHGW) tools (AQUAVEO, 2016).

2.5. Statistical analysis

Multivariate statistical techniques such as Q-mode hierarchical cluster analysis (Q-mode HCA) and Q-and R-mode factor analysis (Q-mode FA and R-mode FA) were used for interpretation of the distinct groups of groundwater, as well as for thes patial hydrochemical processes which may be associated with RW contribution. Euclidean distance was selected for similarity among the transformed data while Ward's linkage method (Ward, 1963) was chosen as the optimal classification parameter. The statistical procedures were applied using the software STATISTICA version 12 (Statsoft Inc., 2013). The data preparation is based on the approach used by Cloutier et al. (2008). The analysis constituted a data matrix of 58 samples by twelve variables. These parameters include pH, hardness, major constituents Ca^{2+}, Mg^{2+}, Na^+, K^+, Cl^-, HCO_3^-, NO_3^--N, SO_4^{2-} and PO_4^{3-}P, as well as

minor constituents Br^-. Boron and water stable isotopes were excluded because they recorded a low communality (of less than 0.5), and their variance is not shared with the other variables. Descriptive and non-parametric (Kurskal-Wallis) statistical tests were used to summarize and compare chemical data between the clusters. If the null hypothesis (H_0 = there is no differences between groups) was rejected, the non-parametric Mann-Whitney *U* test was used to detect differences between specific groups. In addition, the regional distribution of the clustered samples was considered.

Q-and R-mode FA were employed to test the reliability of the different processes (Ledesma-Ruiz et al., 2015; Singh et al., 2004) and to evidence the effect of RW in the groundwater geochemistry. Principal component was selected as the extraction method, whilst the Varimax rotation was applied to reduce the contribution of variables with minor significance facilitating the interpretation of the extracted factors (Yidana et al., 2010). The scree plot and the Kaiser criterion (Kaiser, 1960) were used to determine the optimum number of factors to retain and the validation of the FA was tested by the Kaiser-Mayer-Olin (KMO) (Dimitrov, 2012; Hair et al., 2010).

2.6. Geophysics

In order to assess the flow of RW within the subsoil along the Las Ánimas creek, five electrical resistivity tomography (ERT) lines were measured across the riverbed, starting at the discharge site and ending near the coast (Fig. 1b). Two of these lines were also studied in 2011, prior to RW discharge (Daesslé et al., 2014) and used for comparison. The new measurements were performed in October 2016, using Dipole-Dipole, Schlumberger and Wenner arrays with 28 electrodes spaced 10 m apart, forming a total length of 270 m for each ERT line. Depending on the noise level, Schlumberger and/or dipole–dipole and/or Wenner were tried (even reverse dipole–dipole). This way, the quality of the data and the model were assured. In one case the ERT line was overlapped by 90 m in a roll-along scheme in order to obtain a total length of 450 m. The electrical resistivity measurements were performed using a SUPER STING R1/1P resistivity equipment.

The joint inversion of the mixed resistivity data was performed with the method developed by Pérez-Flores et al. (2001) using their software and 2D resistivity images were produced.

3. Results

3.1. Spatial data interpolation

Based on the cross-validation indicators, Ordinary Kriging provided the best interpolation maps of the SPI, TDS data and water table, with a coefficient of determination r^2 between the predicted and measured values of 0.85, 0.60 and 0.92, respectively. Water levels in 2016 ranged from −8 to 21 m above mean sea level (masl) with a general groundwater flow direction from the coast and downhill along the riverbeds to the central section of the aquifer near the riverbeds, where two depression cones are located (Fig. 2). The spatial distribution of the data is used to support the hydrochemical interpretations.

3.2. Aquifer hydrochemistry

Statistical analyses of the chemical composition in the water sampled throughout the aquifer in April 2016 are presented in Table 1. The ANOVA test ($p < 0.01$) shows statistically significant heterogeneity of the water quality, except in temperature, HCO_3^- and B^-. TDS concentrations are 1080–26,950 mg/L, indicating the presence of brackish (1000–10,000 mg/L of TDS) to saline waters (TDS > 10,000 mg/L). The concentrations of the studied variables in about 80% of the samples are higher than the WHO (2011) guideline values for drinking water and the Mexican guideline of water for human consumption NOM-127-SSA1-1994 (DOF, 2001). Hardness of groundwater exceeds the permissible limit of 500 mg/L (except samples 242 and 3) and is classified as very hard (Sawyer and McCarty, 1967). Concentrations of NO_3^--N range from 0.01 to 49.5 mg/L (average 11 mg/L) and almost half of the samples fall above the limit for drinking water of 10 mg/L.

The significant correlation coefficients ($p < 0.01$) between the transformed parameters are given in Table 2. The correlation of EC, hardness and TDS with Na^+, K^+, Ca^{2+}, Mg^{2+}, SO_4^{2-}, Cl^-, and Br^- as well as among these variables are the highest and their coefficients of determination are significant ($r^2 > 0.7$). The pH is negatively correlated with the aforementioned variables ($r^2 \approx 0.5$) and NO_3^--N is only positively correlated with HCO_3^- ($r^2 = 0.38$).

The cluster analysis results obtained from the HCA for the April 2016 samples classified the groundwater into three distinct groups within the aquifer at $D_{link}/D_{max} < 30$ (Fig. 3). Stiff diagrams for each cluster based on the average values are also presented in Fig. 3. Differences between the three groups are significant (Table 3) and are delimited geographically (Fig. 2). Cluster C1 (in blue) is mostly characterized by the lowest mean values and includes ten wells distributed adjacent to the upper part of the creeks, where the aquifers is recharged and TDS < 1500 mg/L. The freshwater end-member LAC is also included in C1. Cluster C2 (in yellow) correspond to samples with TDS 1500–5000 mg/L and likely represent mixing between C2 and C3 compositions. The three RW samples from the different campaigns are included in C2. Stiff diagrams for C2 and RW have similar shape with the dominant ions. The last cluster (C3, in red) consists of groundwater closest to the coast with the highest TDS > 5000 mg/L.

The results from varimax rotated factor analysis are similar to those from cluster analysis and indicate three factors (F1, F2 and F3) accounting for 86% of the total variance (Table 4). F1 accounts for 60% of the variance and associates hardness, Na^+, Ca^{2+}, Mg^{2+}, Cl^-, SO_4^{2-} and Br^-, which reflect mineral water reactions influenced mainly by seawater intrusion. Factor 2 (16% of the variance) groups K^+ and PO_4^{3-}P with significant loadings in RW and sample 170, and F3 (11% of the variance) has significant loadings for NO_3^--N and HCO_3^- and includes those samples with high nitrate concentrations (> 18 mg/L NO_3^--N).

TDS concentrations between 1500 and 5000 mg/L are commonly found in the aquifer and the lowest TDS concentrations are restricted to some areas upstream of the creeks (Fig. 2). Dominant hydrochemical facies (Fig. 4) are Ca-Na-Cl types, with 20% of bicarbonates of the total anionic mass balance. Similar facies are found in the upper parts under the direct influence of the creeks, but with higher bicarbonate content (~40%). Groundwater near to the coast is characterized by a higher salinity (TDS > 5000 mg/L) and is of Na-Cl composition, with HCO_3^- < 10%. The freshwater end-members well 242 and the surface water have Ca-Na-HCO_3 and Ca-Na-Cl compositions, respectively. Two groundwater samples (3 and 249) taken from Daesslé et al. (2005) indicate that groundwater in the upper part of the San Carlos creek used to be Na-Cl-HCO_3. The water composition of the Punta Banda and the Agua Caliente Submarine hot springs (Vidal-Lorandi and Vidal-Lorandi, 2003) are also considered, showing Na-Cl and Ca-Na-HCO_3 types, respectively.

The effluent water from the discharge sites is characterized by TDS of 2000–3500 mg/L and hardness of 850–1130 mg/L of $CaCO_3$. Boron, K^+ and PO_4^{3-}P in RW are found to be 2×, 5× and 200× higher than the average local concentrations in groundwater, respectively (Table 1). Only B^- in three samples (85, 112 and 160) and K^+ in sample 170 have similar concentrations with respect to RW. Samples 160 and 170 are located in the coastal area, with the highest TDS of 14,190 and 26,950 mg/L, respectively; while sample 85 and 112 are nearby the creeks where discharges with RW take place. The moderate variability of the major ion proportions in the different RW samples exhibit a comparable Na-Ca-Cl composition (Fig. 4), although the slightly more mineralized RW collected in April 2016 shows a Ca-Na-Cl type.

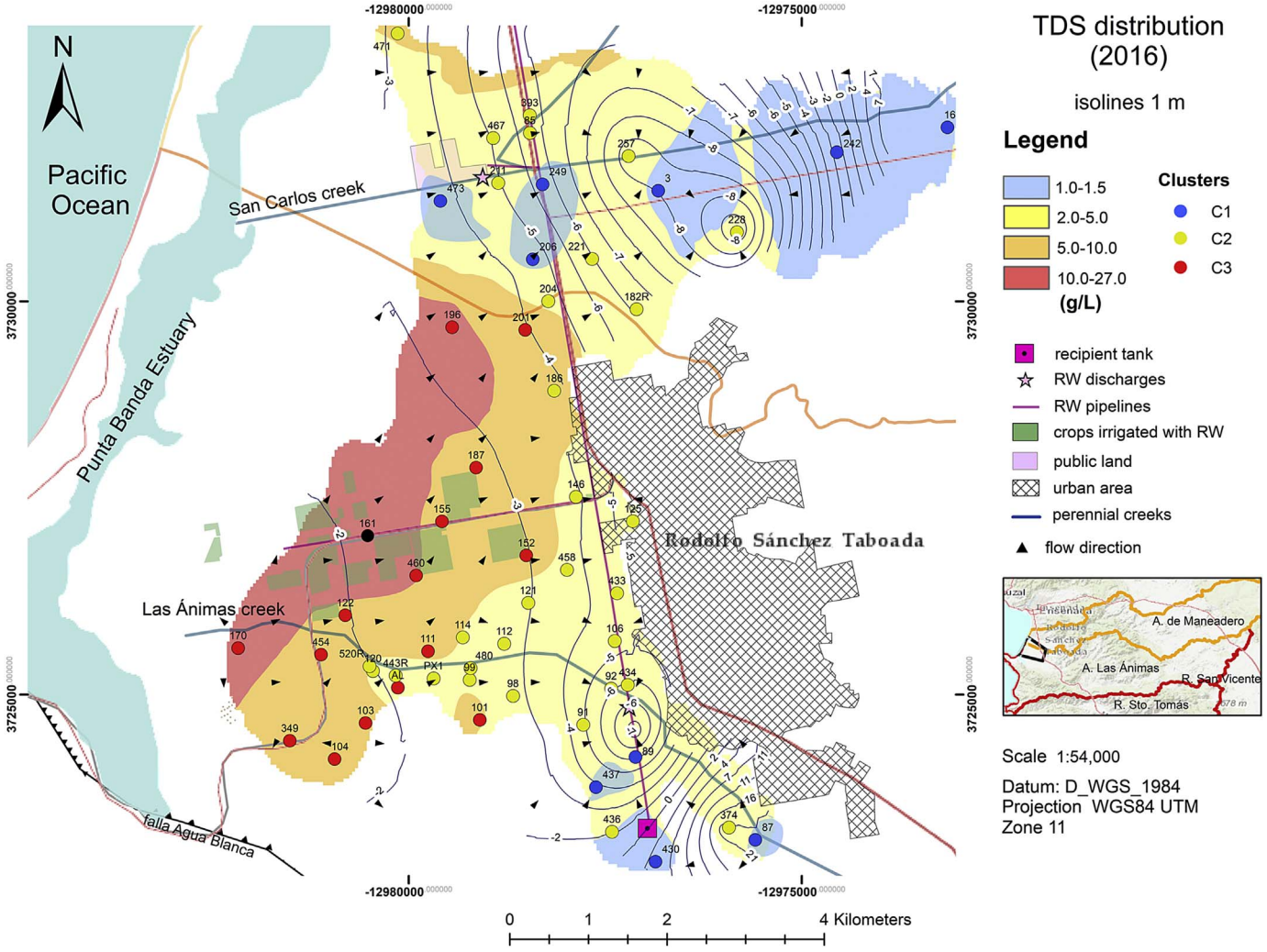

Fig. 2. Regional distribution of the TDS and the clusters from the Q-mode HCA in April 2016. The *isolines* indicate the water level.

3.3. Ionic ratios and cross-plots

In order to identify the interactions between groundwater and RW, the Na-Cl-Br-B systematics (Fig. 5) are used in binary mixing curves as molar ratios. The use of Cl/Br ratios to identify groundwater influenced by RW and other potential sources of salinization is based on the analyzed RW and end-member fields published elsewhere (Alcalá and Custodio, 2004, 2008; McArthur et al., 2012; Panno et al., 2006 and references therein). The Cl/Br vs. Cl^- scatter diagram appears to reflect the trends of mixing as chloride concentrations increase from background levels to the levels found in the sources (Fig. 5a). For the groundwater samples from April 2016, samples with Cl^- concentrations between 300 and 700 mg/L show an increase of Cl/Br molar ratios (i.e. lower dissolved Br^-) and plot within the urban wastewater influence field. Then, samples with $Cl^- > 700$ mg/L overlap the end-member domains of animal and human waste (leaching of solid waste and urban wastewater) and marine intrusion, having high concentrations of nitrates (up to 49 mg/L NO_3-N). The RW molar ratios plot close to those reported for urban wastewater and some samples present values similar to the RW effluent at Las Ánimas creek. Only five samples (460, 187, 196, 170 and 161) plot within the end-member values for seawater intrusion.

A second approach to assess the sources of water is by comparing B/Cl with Br/Cl ratios (Fig. 5b). Groundwater samples with B/Cl ratios higher than seawater ($> 0.74 \times 10^{-3}$) plot either within the hydrothermal field or are in the transition field between seawater intrusion and hydrothermal waters. Only few samples plot within the agriculture drainage field. RW has a B/Cl ratio of 2.3×10^{-3} and plots in the hydrothermal field, similarly to the groundwater from the upper part of the San Carlos creek. Groundwater adjacent to the Las Ánimas creek also appears to be related to hydrothermal waters; except for sample 430 for which B/Cl ratio is closer to seawater. The groundwater samples with lower B/Cl lower ratios ($< 0.74 \times 10^{-3}$) show a trend towards seawater intrusion.

The relationship between Na/Cl ratios relative to Cl^- is often used to identify the mechanism for groundwater salinization (Dixon and Chiswell, 1992; Sappa et al., 2015; Taheri et al., 2017). The molar ratios of the saline groundwater are compared to the theoretical mixing combinations of the seawater (0.86), RW (0.72–0.78) and the LAC (0.46). Most of the samples have Na/Cl ratios lower than seawater and some lower than the LAC (except for three samples with the lowest TDS concentrations), decreasing to 620 mg/L of Cl^- ($f_{SW} < 0.02$) followed by ratios between 0.36 and 0.75 regardless the increase in Cl^- concentrations (Fig. 5c). The Na/Cl ratios in the different RW samples approach those in the groundwater, including those wells nearby the Las Ánimas creek. Variations in the positive chloro-alkaline indices (CAI-1 and CAI-2) and negatives ΔNa (Table 1) indicate that reverse ion exchange is the main process contributing to sodium, with greater Na^+ depletions in the samples that present higher exchange index.

Table 1
Statistical summary of the hydrochemical and isotopic data of seawater (from Appelo and Postma, 2005; Wolfsberg et al., 2009), RW (± standard deviation), the LAC and groundwater from selected wells (n = 57) from April 2016. Wells location in Fig. 1a.

	WHO (2011)	NOM-127 (DOF, 2001)	Mean	Min	Max	SD	ANOVA ($p < 0.01$)	LAC	RW[a]	RW[b]	RW[c]	RW[d]	SW
									Nov 2015	April 2016	August 2017	August 2017	
pH	7–8.5; 9.2	6.5–8.5	7.1	6.6	7.7	0.2	0.00	7.4	7.0	7.2 + 0.1	6.8 ± 0.6	7.6 ± 0.2	8.1
EC (µS/cm)			6307	1438	38,574	6043	0.00	562	4885	3982 ± 1143	4671 ± 455	4432	45,000
TDS (mg/L)	500–1500	1000	4466	1080	26,950	4221	0.00	470	3017	2691 ± 621	2886 ± 76	3663 ± 1088	35,000
Temperature (°C)			21.6	19.9	25	1.1	0.03	14.4	27.7	24.2 ± 0.76	26.9	22.4	20
Hardness ($CaCO_3$ mg/L)	100–500	500	1947	484	6873	1307	0.00	307	889	1057 ± 113	915 ± 61	870 ± 222	6520
Na^+ (mg/L)	50–200	200	846	80	7903	1134	0.00	60	440	437 ± 363	536 ± 56	491 ± 155	11,150
K^+(mg/L)	12		5	3	21	3	0.00[e]	4	23	27 ± 1.8	25 ± 3	21 ± 4	414
Ca^{2+}(mg/L)	75–200		428	130	1131	2493	0.00	78	215	255 ± 29	223 ± 17	210 ± 55	415
Mg^{2+}(mg/L)	50–150		214	34	1097	180	0.00	27	86	102 ± 10	87 ± 4	84 ± 21	1339
Cl^-(mg/L)	200–600	250	2315	290	16,191	2577	0.00	203	1005	1282 ± 105	1084 ± 32	981 ± 297	20,066
HCO_3^-(mg/L)			311	162	441	53	0.02	110	270	398 ± 27	401 ± 26	448	147
CO_3^{2-}(mg/L)			153	80	217	26	0.02	54	133	196 ± 13	197 ± 13	220	72
SO_4^{2-}(mg/L)	200–400	400	370	92	2071	296	0.00[e]	41	219	296 ± 32	240 ± 6	217 ± 49	2815
NO_3^--N (mg/L)	10	10	11.4	0	49.7	12.7	0.02			3 ± 0.25			7×10^{-5}
Br^-(mg/L)	6		6.1	0.90	54.1	8.7	0.00[e]	0.68	2.0	2.3 ± 0.15	2.3 ± 0.46	2.1 ± 0.34	67.3
B^-(µg/L)	500		417	N.D.	836	189	0.04			878			4500
PO_4^{3-}P (µg/L)			30	19	110	13	0.00[e]			5140 ± 90			
$\delta^{18}O$ (‰)			−5.6	6.6	−3.1	0.60	0.00	−6.0	−6.1	−6.8 ± 0.33	−5.8 ± 0.08	−5.5 ± 0.01	0.0 ± 1
δ^2H (‰)			−38.7	−45.6	−23.88	3.7	0.00	−38.2	−41.6	−48.7 ± 2.4	−41.5 ± 0.35	−40.2 ± 0.07	0.0 ± 5
d-excess (‰)			6.0	0.9	9.7	1.4	0.00	10.1	7.5	5.9 ± 1.4	5.2 ± 0.3	4.1 ± 0.1	−5.0
Na/Cl			0.57	0.27	0.94	0.94	0.01	0.46	0.78	0.72 ± 0.08	0.76 ± 0.08	0.77 ± 0.01	0.86
Br/Cl ($\times 10^{-3}$)			1.0	0.59	1.7	0.21	0.00	1.5	0.87	0.81	0.84	0.86	1.5
B/Cl ($\times 10^{-3}$)			1.4	N.D.	6.6	1.5	0.00			2.3			0.74
Ca/(HCO_3 + SO_4^{2-})			1.6	0.80	3.2	0.6	0.00	1.4	1.2	1.0 ± 0.10	1.0 ± 0.05	0.90 ± 0.16	0.35
ΔNa			−18.0	−78.6	1.2	17.7	0.00[e]	0	0.09	−2.7 ± 1.9	−0.7 ± 2.4	−0.2 ± 0.46	0
Δ(Ca + Mg)			18.5	−0.24	59.5	13.0	0.00[e]	0	6.6	8.2 ± 1.9	6.6 ± 1.1	6.4 ± 2.6	0
CAI-1			0.43	0.09	0.72	0.12	0.00	0.53	0.20	0.26 ± 0.1	0.22 ± 0.1	0.21 ± 0.01	
CAI-2			1.96	0.09	6.06	1.34	0.00	1.09	0.62	0.74 ± 0.2	0.58 ± 0.2	0.49 ± 0.1	
f_{SW}			0.10	0.003	0.80	0.13	0.00[e]	0	0.04	0.05 ± 0.01	0.04	0.04	1
Ca/(Ca + Na) (%)			44	12	68	9	0.00	60	33	33 ± 5	32 ± 1	33 ± 1	4
SI_D			0.51	−0.20	1.74	0.44	0.04	−0.68	0.24	0.94 ± 0.15	0.22 ± 0.94	1.5 ± 0.01	0.93
SI_C			0.27	−0.14	0.87	0.21	0.21	−0.26	0.13	0.49 ± 0.08	0.13 ± 0.46	0.80	0.05
SI_A			−1.2	−1.8	−0.55	0.26	0.00	−2.2	−1.4	−1.3 ± 0.06	−1.4 ± 0.03	−1.4 ± 0.02	−0.82
SI_G			−0.94	−1.55	−0.33	0.26	0.00	−1.9	−1.2	−1.0 ± 0.06	−1.1 ± 0.03	−1.2 ± 0.03	−0.60
SI_H			−4.8	−6.06	−2.7	0.72	0.00	−6.6	5.0	−4.8 ± 0.09	−4.9 ± 0.05	−5.0 ± 0.02	−2.5

SD standard deviation; *EC* electrical conductivity; *TDS* total dissolved solids; f_{SW} sweater fraction; *SI*saturation index and subscripts lowercase letters: D = dolomite, C = calcite, A = anhydrite, G = gypsum and H = halite.
N.D. no detected.
[a] RW sampled at the San Carlos creek discharge point.
[b] RW sampled at Las Animas creek discharge point.
[c] RW sampled from the discharge at an irrigation pond.
[d] RW sampled along the RW-flooded Las Ánimas creek.
[e] Calculated by the *Kruskall-Wallis* test.

3.4. Water stable isotopes ($\delta^{18}O_{H2O}$ and δ^2H_{H2O})

The studied waters ranged between −6.6 and −3.1‰ for $\delta^{18}O$ and from −45.6 to −23.9‰ for δ^2H. The surface water at LAC has a $\delta^{18}O$ of −6.0‰ and a δ^2H of −38.2‰; while RW has the most negative values for April 2016 of −6.8 ± 0.33 for $\delta^{18}O$‰ and −48.7 ± 2.4‰ for δ^2H, compared to those RW samples from November 2015 and August 2017 (Table 1). The deuterium excess (*d*-excess defined by Dansgaard (1964) as $d = \delta^2H_{H2O} - 8x\delta^{18}O_{H2O}$) for groundwater ranges from 0.9 to +9.7‰ and decreases as $\delta^{18}O$ becomes more positive ($r^2 = 0.72$, data not shown). The LAC has a *d*-excess of +10‰ and for April 2016 RW has +5.9 ± 1.4‰, changing over the sampling periods. All groundwater samples deviate from the Global Meteoric Water Line (GMWL; Craig, 1961), defining a regression line with the equation: $\delta^2H = 6.1x\delta^{18}O$-4.8. The slope of 6.1 of this line defines a positive trend towards seawater, suggesting mixing processes. The RW effluent also tends to lie along the regression line. Only the surface water at LAC and three samples (87, 437 and 430) correspond to the GMWL. The former indicates that evaporation of surface water is of minor importance which is confirmed by the rather large changes in chloride concentrations with small changes in isotope values for most of the samples (Fig. 7a). Only some samples, plotting above a potential mixing triangle, could be explained by some additional evaporation effect. The isotopic composition of Punta Banda geothermal springs (Vidal-Lorandi and Vidal-Lorandi, 2003) falls within the mixing line with seawater and the initial isotopic signature of water before mixing through the intersection between the mixing line and the GMWL ($\delta^{18}O = -7.7$ and $\delta^2H = -51.4$) match to the Agua Caliente hot spring isotopic composition.

3.5. Water mixing models

Combining $\delta^{18}O_{H2O}$ with Cl^- concentrations is often used as conservative tracers to identify the sources that change the isotopic signature of groundwater (Han et al., 2011; Stumpp et al., 2014). If groundwater is mainly related to mixing with seawater, one would

Table 2
Significant correlation coefficient ($p < 0.01$) of major parameters in groundwater (n = 57).

	pH	EC	TDS	Hardness	Na^+	K^+	Ca^{2+}	Mg^{2+}	Cl^-	SO_4^{2-}	Br^-	$\delta^{18}O$	δ^2H	f_{SW}	HCO_3^-	CO_3^{2-}	NO_3^--N
pH	1.00	−0.44	−0.44	−0.51	−0.41	−0.44	−0.53	−0.46	−0.46	−0.43	−0.44			−0.46			
EC		1.00	1.00	0.93	0.97	0.81	0.82	0.97	0.99	0.95	0.98	0.66	0.62	0.99			
TDS			1.00	0.93	0.97	0.81	0.82	0.97	0.99	0.96	0.98	0.66	0.61	0.99			
Hardness				1.00	0.84	0.72	0.96	0.97	0.94	0.85	0.90	0.64	0.60	0.94			
Na^+					1.00	0.79	0.69	0.92	0.97	0.97	0.98	0.65	0.61	0.97			
K^+						1.00	0.61	0.77	0.80	0.79	0.80	0.60	0.55	0.80			
Ca^{2+}							1.00	0.88	0.83	0.72	0.78	0.50	0.45	0.83			
Mg^{2+}								1.00	0.98	0.92	0.95	0.72	0.69	0.98			
Cl^-									1.00	0.96	0.99	0.67	0.62	1.00			
SO_4^{2-}										1.00	0.96	0.67	0.60	0.96			
Br^-											1.00	0.67	0.63	0.99			
$\delta^{18}O$												1.00	0.98	0.63			
δ^2H													1.00	0.63			
f_{SW}														1.00			
HCO_3^-															1.00	1.00	0.38
CO_3^{2-}																1.00	0.38
NO_3^--N																	1.00

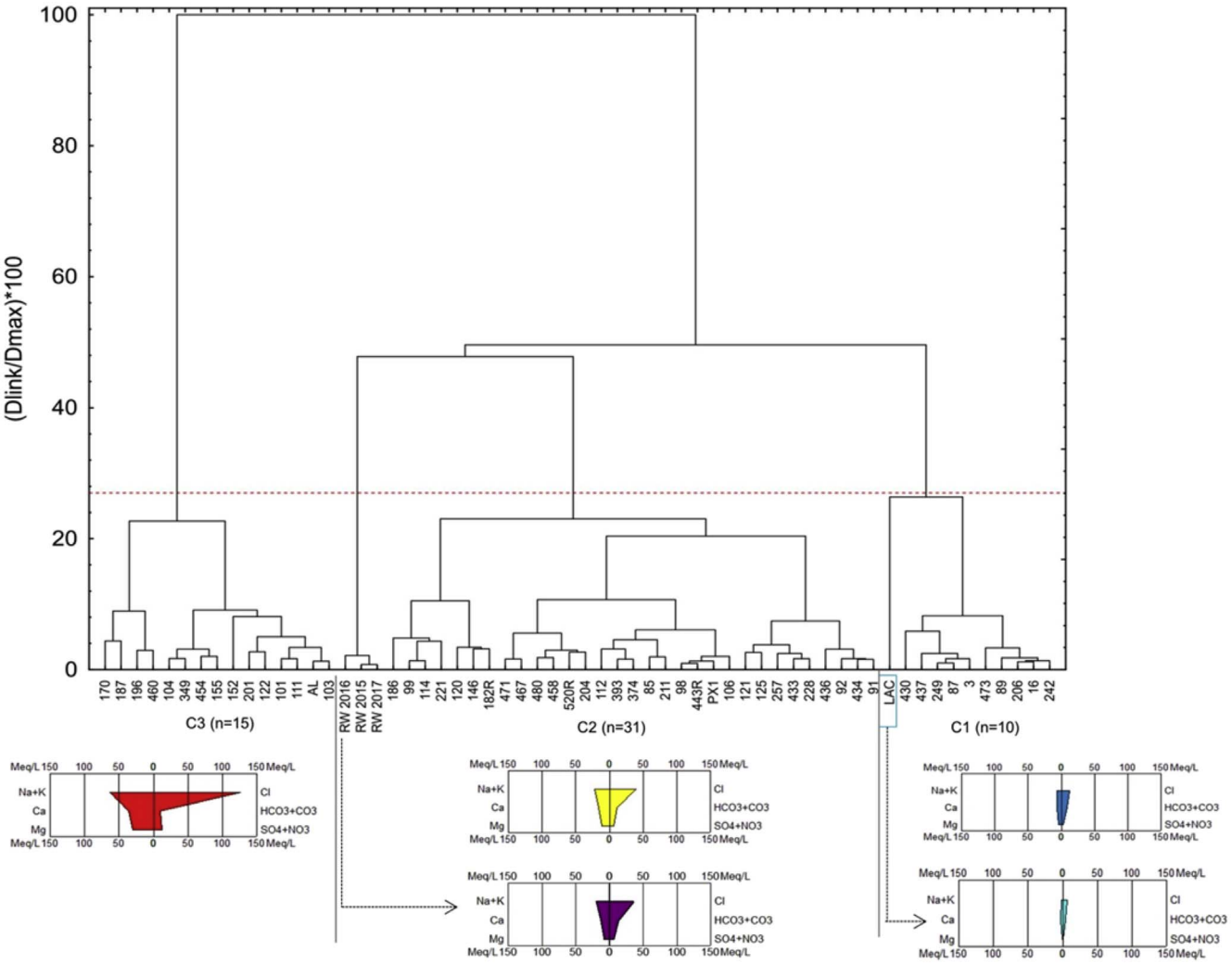

Fig. 3. Dendogram and Stiff diagrams for the groundwater samples (n = 57), and the end-members of the LAC in *light blue* and RW in *purple* from April 2016. (For interpretation of the references to color in this figure legend, the reader is referred to the Web version of this article.)

expect an increase in $\delta^{18}O_{H2O}$ which is concomitant with an increase of Cl^-. For the Maneadero aquifer, the low correlation between Cl^- and $\delta^{18}O_{H2O}$ ($r^2 = 0.45$; Fig. 7a) suggests a mixing of different sources other than seawater. In the Cl-$\delta^{18}O_{H2O}$ diagram, seawater, RW and the LAC are extreme values outside of the observed data to explain the mixture (Christophersen and Hooper, 1992; Phillips and Gregg, 2003). To provide an insight into the RW contribution into groundwater, the Cl^- and $\delta^{18}O_{H2O}$ of the freshwater end-members (242 and the LAC), RW (from the April campaign 2016) and seawater are used as the pair of tracers in Eqs. (1)–(3).

Table 3
Mean values and standard deviations of the hydrochemical parameters of each cluster.

Cluster	C1		C2		C3		*K-W test*
n	10		31		15		$p < 0.01$
	Mean	SD	Mean	SD	Mean	SD	
pH	7.2	0.1	7.1	0.2	6.9	0.2	[a]C3-C1
EC (uS/cm)	1881	287	4204	1396	11,452	3918	0.00
TDS (mg/L)	1332	194	3034	1157	7797	2723	0.00
T (°C)	22.2	1.3	21.2	1.0	21.9	0.8	0.70
Hardness ($CaCO_3$ mg/L)	634	108	1490	452	3436	843	0.00
Na^+ (mg/L)	186	41	516	268	1498	715	0.00
K^+ (mg/L)	3	1	5	1	7	4	0.00
Ca^{2+} (mg/L)	160	25	347	104	739	188	0.00
Mg^{2+} (mg/L)	57	18	152	51	388	101	0.00
Cl^- (mg/L)	435	90	1427	623	4479	1640	0.00
HCO_3^- (mg/L)	266	53	322	43	318	60	[a]C1-C2
CO_3^{2-} (mg/L)	131	26	158	21	157	29	[a]C1-C2
SO_4^{2-} (mg/L)	159	34	293	97	556	203	0.00
NO_3^--N (mg/L)	2.6	3.1	15.9	13.9	8.6	10.5	[a]C1-C2
Br^- (mg/L)	1.0	0.1	3.1	1.6	12.6	6.9	0.00
B^- (µg/L)	464	170	429	181	334	184	0.75
PO_4^{3-}P (µg/L)	44	25	28	4	26	5	[a]C1-C2; C1-C3
f_{SW}	0.01	0.01	0.06	0.03	0.28	0.08	0.00

[a] *Mann-Whitney U* test indicating ONLY significant differences between the two clusters.

Table 4
Varimax rotated R-mode factor matrix.

Variable	F1	F2	F3	Communalities
pH	−0.62	0.08	−0.03	0.40
Hardness	0.97	−0.01	0.00	0.95
Na^+	0.93	0.22	0.18	0.94
K^+	0.40	0.84	−0.02	0.87
Ca^{2+}	0.98	−0.03	−0.01	0.96
Mg^{2+}	0.96	0.00	0.02	0.93
Cl^-	0.96	0.14	0.12	0.96
HCO_3^-	0.16	0.45	0.76	0.80
SO_4^{2-}	0.87	0.18	0.38	0.93
NO_3^--N	0.03	−0.26	0.84	0.77
Br^-	0.97	0.08	0.07	0.96
PO_4^{3-}P	−0.24	0.92	0.00	0.76
Eigenvalue	7.2	1.9	1.3	
% of variance	59.6	15.7	11.0	
% cumulative	59.6	75.3	86.3	

Tracers used for the EMMA based on the PCA include those constitutes that exhibit co-linearity of $r^2 > 0.5$ ($p < 0.01$). Among them are Ca^{2+} and Mg^{2+} (implicit in hardness), Na^+, Cl^-,SO_4^{2-}, Br^- and stable isotopes $\delta^{18}O_{H2O}$ and δ^2H_{H2O}. The two principal components account for 96% of the total variance and most of the groundwater samples are located in the area bound by the end-members (Fig. 7b) and projected similarly as in the Cl-$\delta^{18}O$ diagram. Based on the Rule of One (James and Roulet, 2006), three end-members are acceptable to describe a system. The goodness of fit PCA mixing analysis is based on three criteria described by Christophersen and Hooper (1992): (1) a random pattern of the residuals for each variables against the measured values, (2) regression analysis of $r^2 > 0.90$ between predictions against observations for the original and the orthogonal projections of the end-members and (3) a relative bias ≤15% between the original end-member values and their orthogonal projections. In this study, the first two criteria are achieved (data not shown) supporting the selection of tracers. On the basis of the third criterion, all tracers but water stable isotopes in the LAC and Na^+ and hardness in RW violate the 15% rule. The mixing proportions of RW and seawater from the two EMMA are given in Table 5. The seawater contribution from the two EMMA and the f_{SW} corrected for seawater are identical (± 0.2% difference); while f_{RW} in about 80% of the samples are comparative between the two mixing approaches.

3.6. Synthetic pollution index (SPI)

The SPI has been computed using WHO (2011) values to determine the suitability of groundwater for domestic uses and results are illustrated in Fig. 8. On the basis of SPI, 7% of groundwater samples lie in relatively clean, 67% in lightly polluted and 25% in seriously polluted with all ion species. Only one sample (161) is extremely polluted. Groundwater that is relatively less polluted is distributed adjacent to the upper part of the Las Animas creek; while pollution increases from the center to the coast of the aquifer.

3.7. Temporal changes in hydrochemistry adjacent to the RW recharge site

Temporal variations for Cl^- concentrations, f_{SW} (as indicator of salinity), the molar ratios of Na/Cl and Br/Cl, and the stable isotopes of δ^2H_{H2O} and $\delta^{18}O_{H2O}$ of the groundwater samples collected in November 2015, April 2016, March 2017 and August 2017 are given in Table 6. Groundwater sampled in April 2016 shows higher Cl^- and f_{SW} compared to those in November 2015, except in four samples (257, 99, PX1 and 111), in which salinity is slightly low (760–2883 mg/L of Cl^-) and in sample PX1 about the half to that 2015. Salinity diminishes remarkably after a rainy period in March 2017, except in those wells closer to the coast, probably because seawater intrusion didn't retreat after the rainy period in this highly saline zone of the aquifer. Variations in salinity are reflected in the Na/Cl ratios, showing decreasing ratios with the increasing Cl^- concentrations or vice versa. Yet molar ratios in nine samples (92, 211, 434, 85, 98, 112, 480, 520R and 122) either increase or remain steady with increasing salinity.

On the basis of the Br/Cl ratios, in April 2016 lower ratios ($< 1.5 \times 10^{-3}$) are observed with a slight trend to decrease with increasing in Cl^- to those from 2015, except in two samples (480 and 211) whose ratios increase considerably. Five samples (211, 85, PX1, 98 and 112) taken nearby the LAC present salinities (i.e. $f_{SW} = 0.05$) and molar ratios close to the RW ratio ($0.81–0.87 \times 10^{-3}$). In March 2017, ratios increase (except sample 111) regardless of the shifts in salinity, approaching the value of seawater (1.5×10^{-3}). As for the water stable isotopes, in April 2016 most of the samples show either an increase or decrease regardless the salinity, standing along the mixing line plotted in Fig. 6 compared to those in 2015; while in March 2016 the isotopic signature evolves parallel and above the mixing line. In this period, one sample (89) present the heaviest isotopic composition; while sample 112 results in the most negative isotopic values, even compared to the attributed initial stable isotopes composition of groundwater. Conversely, negligible isotopic variations are observed in sample PX1.

In August 2017, most of the samples evolve to similar hydrochemistry and isotopic composition to those from April 2016. Noticeably, two samples (112 and 111) with lower Cl^- concentrations and higher Br/Cl ratios than those in 2016 show no differences in $\delta^{18}O_{H2O}$ and δ^2H_{H2O}.

3.7.1. Nitrate stable isotopes ($\delta^{18}O_{NO3}$ and $\delta^{15}N_{NO3}$)

Nitrate from different sources is characterized by distinct nitrogen and oxygen isotopic compositions (Xue et al., 2009), and thus, the $\delta^{15}N_{NO3}$ and $\delta^{18}O_{NO3}$ have been used for source identification in this NO_3^--N-rich aquifer. The relationship between $\delta^{18}O_{NO3}$ and $\delta^{15}N_{NO3}$ of the selected wells from December 2016 and March 2017 and the ranges for potential nitrate sources (Kendall et al., 2007; Silva et al., 2002) are shown in Fig. 9. The $\delta^{18}O_{NO3}$ varies from +1.2 to +16.7‰ in December 2016 and decreases from +0.8 to +8.9‰ in March 2017. The $\delta^{15}N_{NO3}$ values range from +3.8 to +85.95‰ in December 2017 and from +4.8 to +22.8‰ in March 2017. The LAC has a $\delta^{18}O_{NO3}$ of +6.8 and a $\delta^{15}N_{NO3}$ of +7.0; while the RW effluent has $\delta^{18}O_{NO3}$ and $\delta^{15}N_{NO3}$

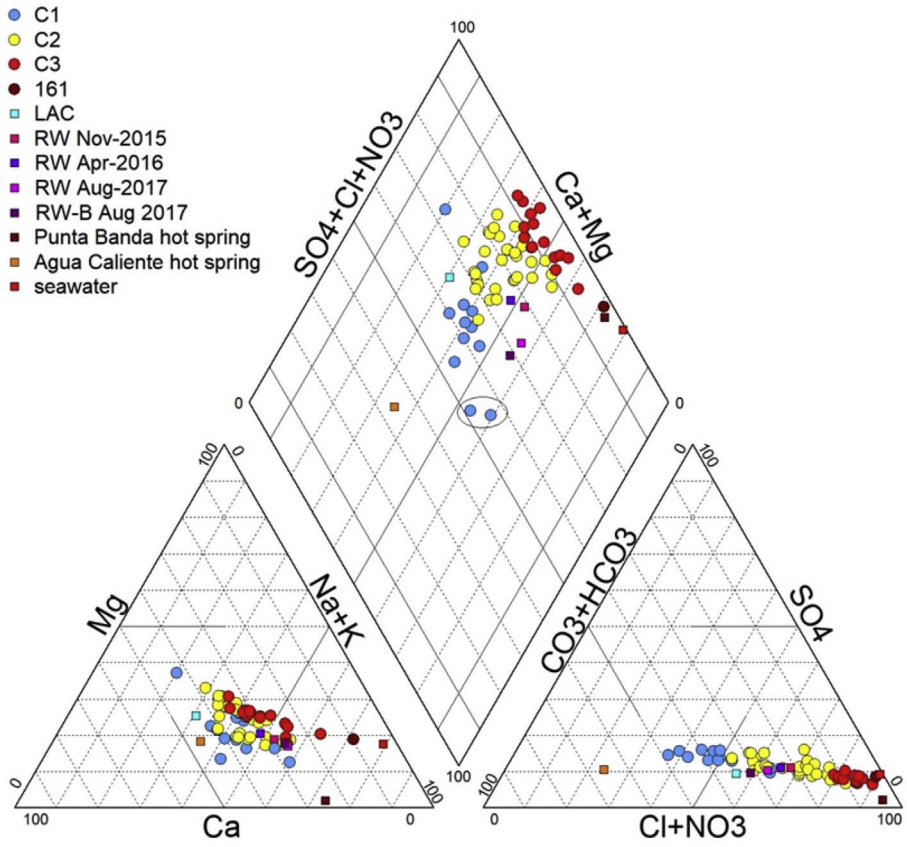

Fig. 4. Piper diagram showing the relative proportions of major ions for the clusters in April 2016, the hot springs of Punta Banda and Agua Caliente (from Vidal-Lorandi and Vidal-Lorandi, 2003) and the end-members of the LAC (surface water of the Las Ánimas creek), seawater and RW. The *enclosed* indicate the proportion of the major ions of wells 3 and 249 (from Daesslé et al., 2014).

values of +12.5‰ and −9.1‰, respectively. For the two sampling campaigns, most groundwater samples are found in the range of wastewater and manure waste, except for a few samples belonging to cluster C1 and C3. Still, mineralization of soil organic matter and nitrification processes cannot be ruled out for some of the samples due to overlapping ranges of $\delta^{15}N_{NO3}$.

3.8. Geoelectrical data

The 2-D resistivity profiles display resistivity values as the base 10 logarithm of the resistivity, and will be refered to based on that scale. The resistivities vary from 0.9 to 2.5 in logarithm scale or from 8 to 316 Ωm in a linear scale, at a maximum depth of 60 m for all surveys (Fig. 10). These values are separated into three fairly uniform layers for each resistivity difference and are shown as blue, green-yellow and orange-red colors. It is observed that the RW discharge point at LAC is causing infiltration of water with resistivities equivalent to 1.5–1.9 logarithm scale (yellow-green), apparently flowing to the south of a more saline barrier that has resistivities of 0.9–1.5 (in orange-red). This lateral displacement fluctuates along the parallel section of the creek towards the south and less so the north of the riverbed, and possibly mixes with groundwater of similar resistivities.

4. Discussions

4.1. Origin of solutes and groundwater mineralization processes

In the Maneadero aquifer, variation in the geochemistry reflects the influences of different sources and geochemical processes. The significant strong correlations of Cl^- with Ca^{2+}, Na^+, K^+, SO_4^{2-}, $Mg^{2+}$and Br^- (Table 2), as well as among these ions indicates that these elements are mostly contributed by mineralization (Bouzourra et al., 2015) and that dissolution of rock minerals and evaporites is the first step in the hydrogeochemical evolution. Their negative correlation with pH suggest that dissolution of these salts is related to some degree to acidic conditions of groundwater (Manno et al., 2006).

Bromide concentrations of 0.9–6.0 mg/L in the upper and central part of the aquifer falls in the range for volcanic rock (Sugiura, 1968) and evaporites (Kabata-Pendias and Pendias, 2001), while higher concentrations (up to 54 mg/L) nearer to the coast coincide with natural brines and thermal waters (Kikkawa and Shiga, 1966). Also, the Cl/Br ratios ≥673 (Fig. 5a) indicate the source as halides (Davis et al., 1998; Vengosh and Pankratov, 1998); thus, Br^- can result from soluble salts and mixture with seawater.

Scapolites and gypsum and/or anhydrite dissolution in the aquifer are probably responsible for correlations of SO_4^{2-} with Ca^{2+}, Na^+ and Cl^-. Similarly, the dissolution of halite of marine aerosols is likely with a correlation r^2 between Na^+ and Cl^- of 0.97. The capacity of groundwater to dissolve these minerals along the flow paths is demonstrated by the under saturation in all facies with respect to halite, anhydrite and gypsum, and its strong trend of being less under-saturated with growing TDS (r^2 = 0.90, data not shown). The Ca/(Ca + Na) molar ratio from 30 to 50% indicates anorthite typical of andesite, which is characteristic of the geology in the region.

Calcium and magnesium directly contribute to hardness and their significant correlation with Cl^- and SO_4^{2-} and among them indicates that hardness of the water is permanent in nature. The dissolution of carbonate minerals is the major source of these ions. Most of the groundwater samples are oversaturated (SI > 0) with respect to calcite (SI_C) and dolomite (SI_D), indicating that water is incapable of dissolving carbonate minerals giving the local physicochemical conditions. The significant correlation between the SI_C and SI_D (r^2 = 0.93, $p < 0.01$; data not shown) evidences that gypsum and/or anhydrite dissolution does not considerably contribute to calcium (Argamasilla et al., 2017). Thus, a removal of Ca^{2+} and Mg^{2+} may occur throughout other processes such as reverse cation-exchange reactions. In addition, the lack of

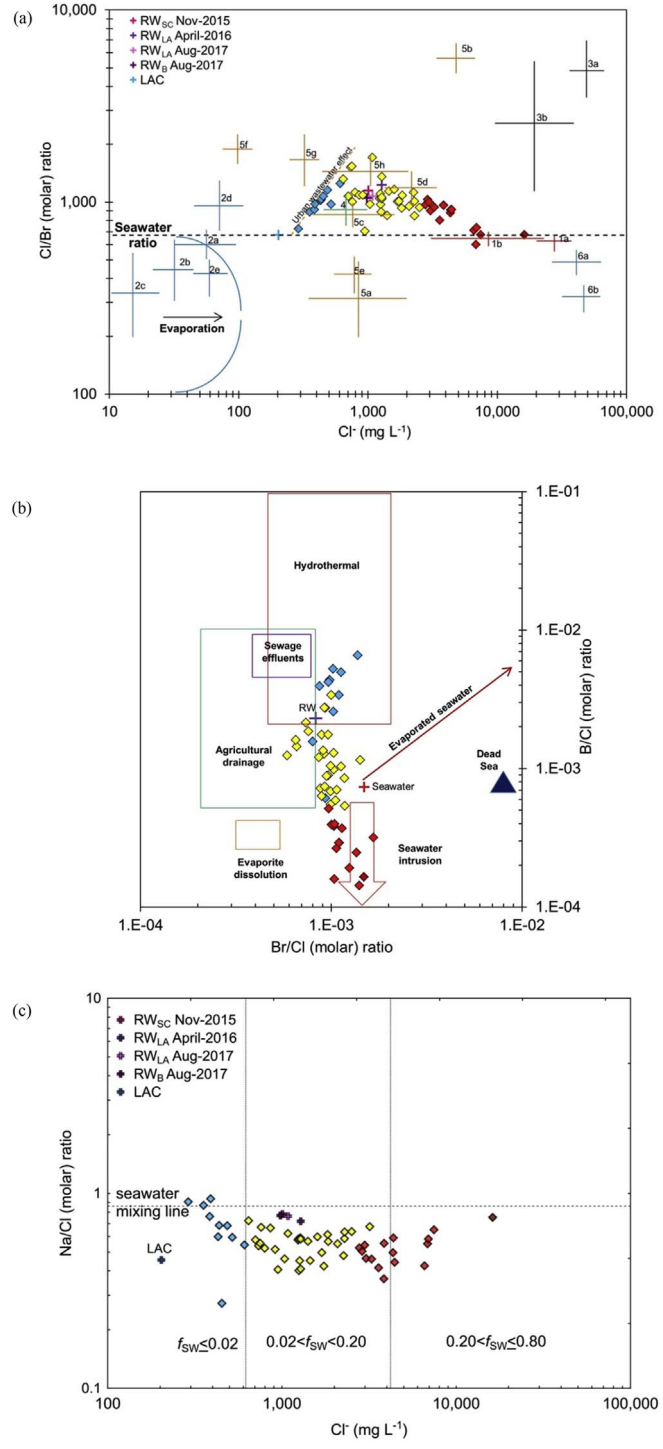

Fig. 5. (a) Cl/Br against Cl^- (modified from Alcalá and Custodio, 2008), (b) Br/Cl against B/Cl (adapted from Vengosh, 2014) and (c) Cl^- against Na/Cl for the clusters in April 2016. Fields are: 1a, seawater brines; 1b, seawater intrusion; 2a, coastal areas; 2b, inland areas; 2c, high altitude/continental; 2d, coastal arid climate; 2e, coastal polluted areas; 3a, leaching of natural halite; 3b, leaching of gypsum containing halite; 4, volcanic halides; 5a, agricultural pollution; 5b, leaching of halite (road salt); 5c, leaching of garbage and solid waste; 5d, urban wastewater, 5e, septic waste; 5f, septic-tank outflow; 5 g, sewage effluent; 5 h, animal waste; 6a, leaching of carnalite; 6b, leaching of sylvite.

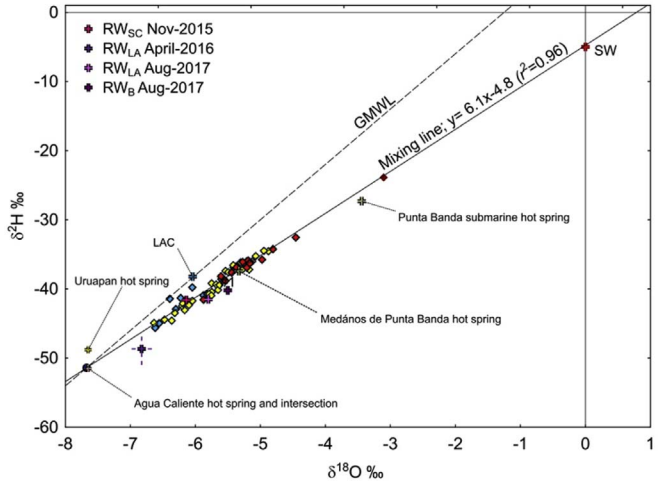

Fig. 6. Relationship between $\delta^{18}O$ and $\delta^{2}H$ for the clusters in April 2016.

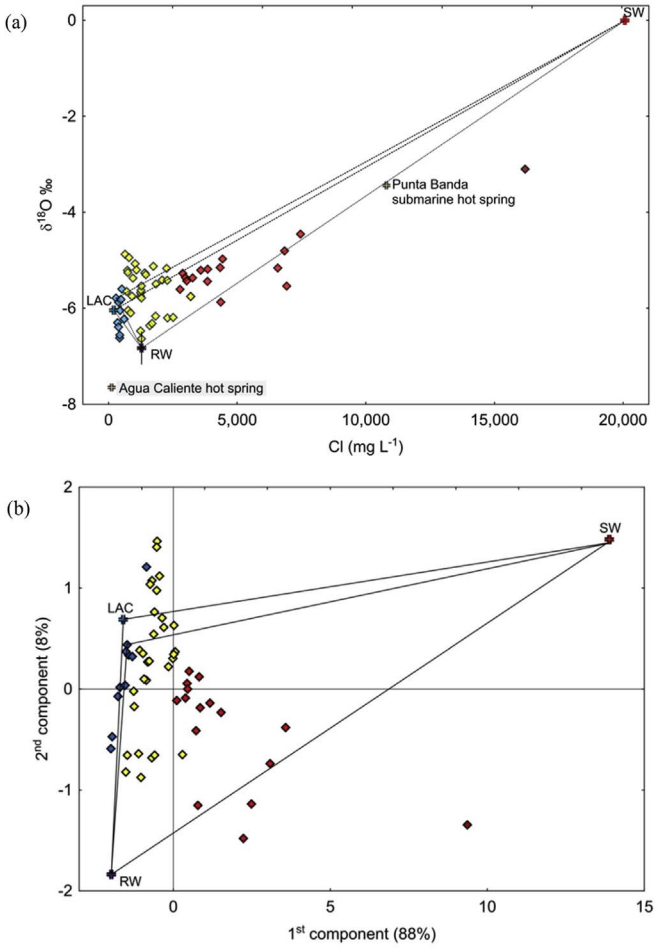

Fig. 7. Three end-member mixing analysis using (a) Cl^- vs. $\delta^{18}O$ and (b) principal component analysis for the clusters in April 2016.

correlation of HCO_3^- with Ca^{2+} and Mg^{2+} and between these ions with SI_D and SI_C (data not shown) indicates sources other than the dissolution of carbonate minerals (Bouzourra et al., 2015). As for HCO_3^-, its negligible variations in groundwater suggest that bicarbonate prevails due to the unconfined nature of the aquifer and the importance role of calcite equilibrium (Martínez and Bocanegra, 2002).

The Na/Cl molar ratios of groundwater from the upper parts of the are ca. 1 and their water composition is Na-Cl-HCO_3 (Fig. 4) as identified by Daesslé et al. (2005). These waters characterize a transition zone and indicate the freshening of the aquifer and the influences of source lithology (Voutsis et al., 2015). Assuming that Na^+ in the groundwater system derives from halite dissolution, the Na/Cl will correspond 1 (Appelo and Postma, 2005; Meybeck, 1987). However,

Table 5
Results of the two EMMA, giving the contribution of seawater (f_{SW}) and RW (f_{RW}) in the groundwater samples. For the two mixing approaches, those samples that fall within the mixing zones are indicated in bold. The $^{*}f_{SW}$ is the seawater contribution corrected for seawater mixing.

Tracers	Cl^-	Cl^- and $\delta^{18}O_{H2O}$		PCA	
EMMA		1st		2nd	
Fractions	$^{*}f_{SW}$	f_{RW}	f_{SW}	f_{RW}	f_{SW}
3	0	0.06	0	0.24	0
87	0.01	0.17	0	0.40	0.01
16	0.01	0.10	0	**0.07**	**0**
206	0.01	0.16	0	0.70	0
249	0.01	0.13	0	0.43	0
430	0.01	**0.07**	**0.01**	**0.18**	**0.01**
89	0.02	0	0.02	0	0.02
437	0.02	**0.28**	**0.01**	**0.36**	**0.01**
473	0.01	**0.05**	**0.01**	**0.06**	**0.01**
91	0.02	0	0.02	0	0.02
228	0.02	0	0.02	**0.04**	**0.03**
433	0.03	0	0.03	0	0.03
434	0.03	0	0.03	0	0.03
257	0.02	**0.23**	**0.01**	**0.21**	**0.02**
92	0.03	0	0.03	0	0.03
182R	0.03	**0.28**	**0.01**	**0.28**	**0.02**
125	0.03	**0.08**	**0.03**	**0.05**	**0.03**
121	0.04	0	0.04	0	0.04
106	0.04	0	0.04	0	0.04
436	0.04	0	0.04	0	0.06
PX1	0.05	**0.02**	**0.05**	**0.36**	**0.05**
211	0.05	**0.57**	**0.02**	**0.49**	**0.02**
443R	0.05	0	0.05	**0.26**	**0.05**
374	0.05	0	0.05	**0.25**	**0.05**
85	0.05	**0.67**	**0.01**	**0.56**	**0.02**
98	0.05	0	0.05	**0.12**	**0.06**
112	0.05	**0.22**	**0.04**	**0.38**	**0.05**
146	0.06	0	0.06	**0.08**	**0.08**
120	0.06	0	0.06	**0.03**	**0.08**
204	0.07	**0.56**	**0.03**	**0.60**	**0.05**
393	0.07	**0.55**	**0.04**	**0.49**	**0.04**
458	0.08	0	0.08	**0.08**	**0.11**
221	0.08	**0.84**	**0.04**	**0.83**	**0.06**
114	0.08	0	0.08	**0.22**	**0.10**
99	0.09	**0.09**	**0.09**	**0.19**	**0.11**
480	0.10	0	0.10	**0.16**	**0.11**
520R	0.10	**0.16**	**0.09**	**0.24**	**0.11**
467	0.10	0.94	0.06	**0.83**	**0.06**
471	0.11	**0.62**	**0.08**	**0.51**	**0.07**
186	0.15	**0.83**	**0.11**	**0.86**	**0.12**
103	0.13	**0.42**	**0.14**	**0.50**	**0.12**
111	0.13	**0.18**	**0.12**	**0.35**	**0.14**
AL	0.14	**0.28**	**0.12**	**0.41**	**0.14**
101	0.14	**0.34**	**0.12**	**0.49**	**0.13**
155	0.15	**0.34**	**0.13**	**0.37**	**0.13**
349	0.17	**0.29**	**0.15**	**0.56**	**0.16**
104	0.18	**0.46**	**0.16**	**0.68**	**0.16**
454	0.18	**0.23**	**0.17**	**0.39**	**0.16**
122	0.21	**0.42**	**0.19**	**0.50**	**0.18**
201	0.21	**0.75**	**0.16**	**0.78**	**0.17**
152	0.21	**0.30**	**0.20**	**0.57**	**0.21**
460	0.32	0.71	0.29	0.74	0.26
187	0.33	**0.55**	**0.30**	**0.66**	**0.32**
196	0.34	0.70	0.30	0.74	0.26
170	0.37	**0.57**	**0.34**	0.66	0.34
161	0.80	0.21	0.79	0.31	0.70

most of the groundwater samples present an overall dominance of Cl^- over Na^+, with low Na/Cl ratios (< 0.86). The depletion of Na^+ is attributed to reverse ion exchange, which is evident from the chloro-alkaline indices (Custodio and Llamas, 1996). The deficit of ΔNa and the excess of Δ(Ca + Mg) relative to the theoretical mixing of freshwater and seawater (Table 1) reinforce even more the occurrence of reverse ion exchange. The inverse relationship of Δ(Ca + Mg) with ΔNa occurs when Ca^{2+} and Mg^{2+} is released while Na^+ is added to the aqueous solution (Tellam and Llyod, 1986; Vengosh, 2003), resulting in elevated concentrations of Ca^{2+} and Mg^{2+} and lower Na^+ concentrations than expected considering the simple halite dissolution and/or freshwater-seawater mixing process (Argamasillaet al., 2017). Reverse ion exchange reactions can be considered as the second step of the hydrochemical evolution responsible for the removal of Ca^{2+} and Mg^{2+} and, as consequence, groundwater exhibits a Ca-Na-Cl composition (Fig. 5) of the seawater plume (Jeen et al., 2001; Vengosh and Benzvi, 1994). The $Ca/(HCO_3+SO_4) \geq 1$ suggests additional source of Ca^{2+} other than reverse cation exchange reactions and according to Daesslé et al. (2014) the excess of Ca^{2+} might derive from the dolomitization of the Upper Cretaceous marine sediments.

Concentrations of dissolved $PO_4^{3-}P$ in groundwater (0.019–0.11 mg/L) are below the standard established for drinking water (i.e. 1.5 mg/L; Singh et al., 2014) but close and above to the USEPA level of ≤0.025 mg/L for prevention of eutrophication in reservoirs (USEPA, 1986). Factors that influence high levels of $PO_4^{3-}P$ in groundwater are usually attributed to the application of fertilizers and the leakage of domestic sewage (Kummar et al.,2009; Sikora et al., 1976; USGS, 1999). Concentration of $PO_4^{3-}P$ in the RW effluent is 5.2 mg/L, i.e. 200× the average concentration of $PO_4^{3-}P$ in groundwater. Phosphate tends to sorb to iron hydroxides and reducing conditions can promote the dissolution of iron oxides, releasing also phosphorus into groundwater (Spiteri et al., 2008). The $PO_4^{3-}P$ in the aquifer of Maneadero is probably attenuated by sorption processes.

4.2. Groundwater classification and factors controlling the hydrochemistry

The R-mode FA validates the groundwater groups defined by the Q-mode HCA and confirmes the findings from the correlation analysis by defining three independent latent factors that are influencing the water quality. Most of the samples of clusters C1 and C2 are located in areas where static water levels range between −8 and −5 masl, whereas cluster C3 is situated close to the coast where static water levels are between −3 and −2 masl. The Cl^- concentrations are therefore related with the proximity to the coast and the level of groundwater extraction.

Cluster C3 describes a water composition of Na-Cl type with seawater mix from 10 to near 40% (Table 3) and its association to F1 reflects mineralization mainly by seawater intrusion. The clusters C1 and C2 are of Ca-Na-Cl type composition, differing only in their percentage of bicarbonates. Cluster C2 has higher TDS concentrations than cluster C1 and is characterized by the highest NO_3^--N throughout. Most of the samples of cluster C2 and some of cluster C3 are grouped in F3, which accounts for NO_3^--N and HCO_3^-. This factor refers groundwater contaminated with nitrates and its relation to HCO_3^- may indicate degradation of organic matter. Finally, the association of $PO_4^{3-}P$ and K^+ in F2 is related only to RW with limited presence in sample 170, probably due to the adsorption of these two ions onto clay minerals.

4.3. Influence of RW and other potential sources on groundwater mineralization

The ratios of Na/Cl < 0.86 decrease as Cl^- concentrations increase, typical of salinization related to seawater intrusion (Najib et al., 2016; Richter and Kreitler, 1993). However, the scattered pattern of the Na/Cl ratios < 0.86 regardless the increases in Cl^- suggest contamination with saline water besides seawater intrusion. The trend displayed by the Cl/Br ratios vs. Cl^- (Fig. 5a) show ratios within the range for water containing dissolved halides related to human and animal waste, which is higher than that of seawater. These deviations demonstrate human activity contribution in groundwater salinization in addition to seawater, which may explain the Na^+ depletions related to reverse-ion exchange reactions. The Cl/Br ratios found in RW overlap with the ratios of urban wastewater and animal waste and, thus, additional hydrochemical tracers were considered to identify the

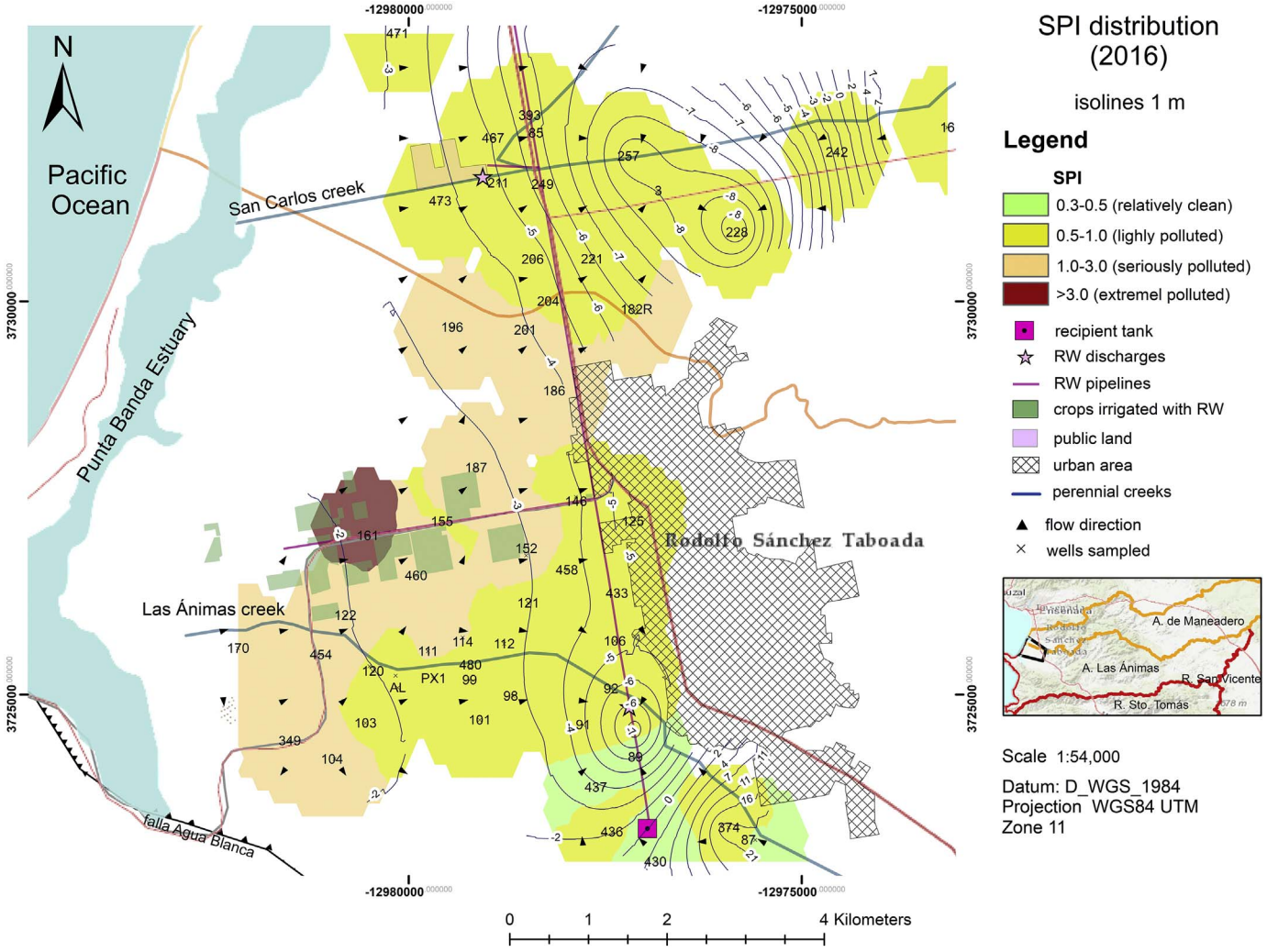

Fig. 8. Regional distribution of SPI values in April 2016. The *isolines* indicate the water level.

fingerprint of the RW effluent.

The comparison between the molar ratios of B/Cl and Br/Cl (Fig. 5b) for different salinity sources revealed the hydrothermal signal of groundwater in the upper part of the creeks. The B/Cl ratios are comparable to those reported for geothermal springs at San Carlos and Punta Banda (Arango-Gavlán et al., 2011) and, thus, are consistent with the hydrothermal source; although for some samples contribution of agricultural drainage and seawater cannot be ruled out. The RW also reflects the hydrothermal signature. This is possible considering that groundwater is returned later as the effluent. However, the relatively high B^- concentration in RW (878 μg/L) is indicative of B^- compounds from bleaching agents (Vengosh and Keren, 1996). Concentrations of B^- in groundwater are lower than RW and far below those recorded in the hydrothermal springs surrounding the study area (7900–9700 μg/L, Arango-Galvan et al., 2011). This indicates that such concentrations result from the adsorption of B^- onto mineral surfaces, which is confirmed by the decrease of B/Cl ratio with increasing Cl^- concentrations. Remarkably, two samples (112 and 85) located close to the discharge points have B^- concentrations and B/Cl ratios similar to RW, suggesting that clay minerals might have reached a steady state with respect to B^-.

The Na/Cl ratios in RW are lower than those reported in treated wastewater in Israel (Vengosh and Keren, 1996; Vengosh, 2014) and comparable to some groundwater samples close to the discharge site at LAC and nearby the urban area (Fig. 5c); thus, this ratio alone cannot be helpful for tracing the RW effluent. However, the variations of Na/Cl ratios over time suggest that reverse cation-exchange reactions occur during the RW or other effluent arrival to the aquifer and once the exchangeable sites become saturated, sodium is not retained from the effluent and behaves conservatively in groundwater (Vengosh and Keren, 1996F). These findings also observed for B^-might indicate the limited capacity of clay minerals to retain these elements.

The potential contribution of seawater estimated from EMMA is consistent with the seawater fractions corrected for seawater and with the spatial variation of the TDS and the Q-mode HCA (Fig. 2). The extent of seawater contribution in most of the aquifer is almost 40% and based on the Na-Cl-Br-B systematics (Fig. 5) groundwater is significantly influenced by anthropogenic-derived processes. This hypothesis is coherent with the observed relationship between Cl^- concentrations and $\delta^{18}O_{H2O}$ (Fig. 7a). The assumption that RW is contributing to groundwater chemistry seems to be supported by the mixing analysis between Cl^- and $\delta^{18}O_{H2O}$ (Fig. 7a) and the mixing model constructed from the PCA (Fig. 7b). In these respect, the plausibility of the chosen end-members is validated by the criterion for the PCA mixing approach. Despite that both mixing models reveal comparable RW mixing proportions, the fractions of RW cannot satisfactory explain the hydrochemistry in the groundwater samples; i.e. samples closer to the source of discharge have geochemical signatures similar to RW, but percentages of RW < 50%. On the contrary, samples with trends to seawater signature (f_{SW} > 8%) have percentages of RW up to 80% (Table 5).

The Rule-of- One supports the contribution of the three end-

Table 6
Comparative groundwater hydrochemistry from November 2015, April 2016, March 2017 and August 2017. Clusters are indicated in parentheses. The f_{SW} is the seawater fraction corrected for seawater mixing.

Well ID	November 2015						April 2016						March 2017						August 2017					
	Cl^- (mg/L)	Na/Cl	Br/Cl ($\times10^{-3}$)	$\delta^{18}O$ (‰)	$\delta^{2}H$ (‰)	f_{SW}	Cl^- (mg/L)	Na/Cl	Br/Cl ($\times10^{-3}$)	$\delta^{18}O$ (‰)	$\delta^{2}H$ (‰)	f_{SW}	Cl^- (mg/L)	Na/Cl	Br/Cl ($\times10^{-3}$)	$\delta^{18}O$ (‰)	$\delta^{2}H$ (‰)	f_{SW}	Cl^- (mg/L)	Na/Cl	Br/Cl ($\times10^{-3}$)	$\delta^{18}O$ (‰)	$\delta^{2}H$ (‰)	f_{SW}
3 (C1)	259	0.86	1.5	−6.7	−43.5	0	355	0.87	1.1	−6.3	−42.9	0												
87(C1)							385	0.76	1.1	−6.4	−41.4	0.01	723	0.68	1.4	−4.8	−32.3	0.03						
89 (C1)							519	0.59	1.0	−5.6	−38.6	0.02	790	0.41	1.5	−6.1	−39.3	0.03						
92 (C2)	558	0.64	1.0	−4.9	−32.8	0.02	796	0.52	0.89	−4.9	−34.5	0.03	846	0.63	1.2	−5.3	−36.0	0.03	768	0.65	0.97	−5.0	−35.7	0.03
211 (C2)	955	0.57	0.76	−6.8	−44.6	0.04	1247	0.58	0.91	−6.5	−44.4	0.05												
434 (C2)	546	0.68	0.92	−5.0	−34.6	0.02	750	0.56	0.65	−5.3	−36.3	0.03	783	0.66	1.4	−5.1	−34.3	0.03	651	0.76	0.75	−5.4	−36.8	0.01
85 (C2)	1173	0.51	1.0	−6.5	−43.3	0.05	1278	0.59	0.96	−6.6	−44.9	0.05												
257 (C2)	785	0.69	0.84	−6.3	−42.4	0.03	760	0.67	1.0	−6.0	−41.7	0.02												
112 (C2)	1212	0.55	0.81	−5.8	−38.7	0.05	1280	0.58	0.74	−5.8	−40.7	0.05	592	0.81	1.1	−10.5	−74.0	0.02	832	0.60	0.99	−5.8	−39.9	0.03
374 (C2)							1264	0.45	1.1	−5.6	−39.4	0.05	1101	0.48	1.4	−6.0	−38.9	0.05						
PX1 (C2)	2325	0.38	0.87	−4.8	−33.5	0.11	1237	0.58	0.96	−5.7	−40.5	0.05	1047	0.64	1.3	−5.9	−40.5	0.04	1276	0.62	1.0	−5.7	−39.9	0.05
98 (C2)							1279	0.41	0.94	−5.5	−37.4	0.05	1363	0.49	1.3	−5.3	−36.1	0.05	1740	0.48	1.0	−5.2	−35.8	0.08
120 (C2)							1451	0.45	0.88	−5.3	−36.2	0.06	2122	0.62	1.2	−5.5	−36.7	0.10						
480 (C2)	1467	0.46	0.66	−5.6	−37.6	0.06	2259	0.48	0.89	−5.2	−37.2	0.10	1822	0.46	1.1	−5.6	−38.0	0.08	2073	0.43	1.1	−5.4	−37.8	0.09
99 (C2)	2157	0.31	0.86	−5.3	−35.5	0.10	2084	0.55	1.1	−5.4	−36.9	0.09	1866	0.54	1.1	−5.7	−39.6	0.08	1105	0.62	1.0	−5.5	−38.8	0.05
114 (C2)							1845	0.57	0.92	−5.5	−37.6	0.08	2065	0.48	1.3	−5.7	−40.2	0.09	2095	0.56	0.96	−5.4	−37.2	0.10
111 (C3)	2976	0.45	0.91	−5.1	−33.7	0.14	2883	0.50	0.97	−5.3	−36.1	0.13	2184	0.57	0.47	−5.5	−38.2	0.10	1835	0.52	1.1	−5.4	−37.7	0.08
520R (C3)							2285	0.59	1.2	−5.4	−36.6	0.10	2355	0.61	1.1	−5.5	−37.7	0.11						
101 (C3)							3042	0.46	1.1	−5.4	−37.5	0.14	2827	0.51	1.2	−5.4	−37.7	0.13	3243	0.39	1.1	−5.2	−36.1	0.15
454 (C3)							3855	0.55	1.0	−5.2	−35.9	0.18	2870	0.67	1.2	−5.3	−36.4	0.13	3652	0.47	1.0	−5.2	−36.0	0.17
122 (C3)							4338	0.50	1.1	−5.2	−36.1	0.21	4631	0.65	1.2	−4.8	−33.9	0.22						

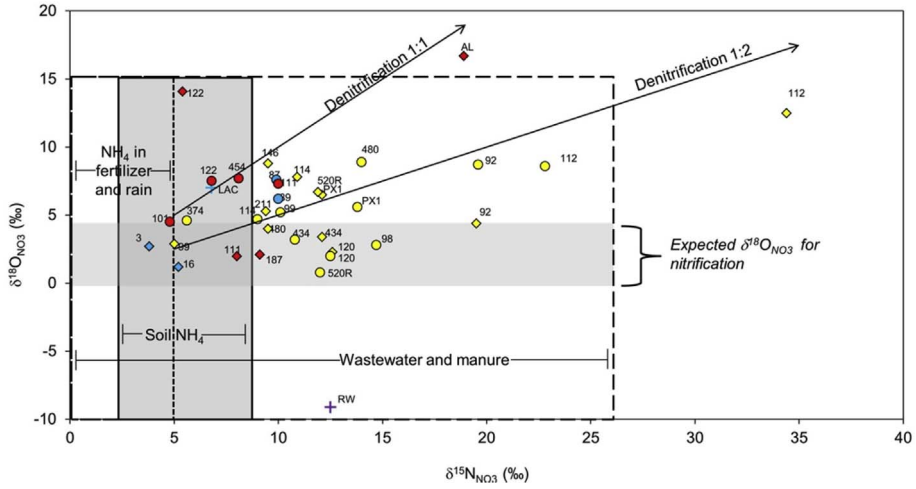

Fig. 9. Bivariate plot of $\delta^{18}O_{NO3}$ and $\delta^{15}N_{NO3}$ for the groundwater clusters in Maneadero. The *rhomboid symbols* are from December 2016 and the *circle symbols* are from March 2017. The isotopic composition of various nitrate sources are also shown (adapted from Kendall et al., 2007).

members in explaining almost all the variability, but the projection of the samples in the mixing spaces (Fig. 7a–b) indicates that additional end-members are contributing to the groundwater chemistry. On the basis of the third criterion for the PCA mixing approach, Cl^- and water stable isotopes have the smallest relative bias and below the 15% threshold for all end-members. This indicates that the conservative behavior is most appropriate for these solutes. In the case of the other variables, the relative bias > 15% in the LAC and Na^+ and hardness in RW either suggest that they do not adhere with physical mixing control or are not mixing with the same ratios (James and Roulet, 2006). In addition, freshwater derived from the LAC may not directly interact with many sites. Because the LAC and seawater have a unique and extreme geochemical and isotopic signature, it was possible to estimate their contribution in groundwater. Contrary, the over- and under-estimates of RW contribution is suggestive of missing end-members, probably with similar geochemical signatures to RW. This is possible considering that the source of reclaimed water is mainly urban wastewater and that some parameters such as TDS, B^- and Br^- are not removed from the treated effluent.

The use of isotopes to estimate the contribution of sewer effluents has successfully been applied on relatively small catchment areas with simple geohydrological groundwater where water is not harvested from the local aquifer and later returned as RW (Schilperoort et al., 2007). The integration of the potential end-members together with other solutes (e.g. boron isotopes), however, could provide more information to its relative contribution in groundwater. The RW effluent is a mixture of seawater and different water sources which have experienced several transitions, leading to changes in its geochemical and isotopic

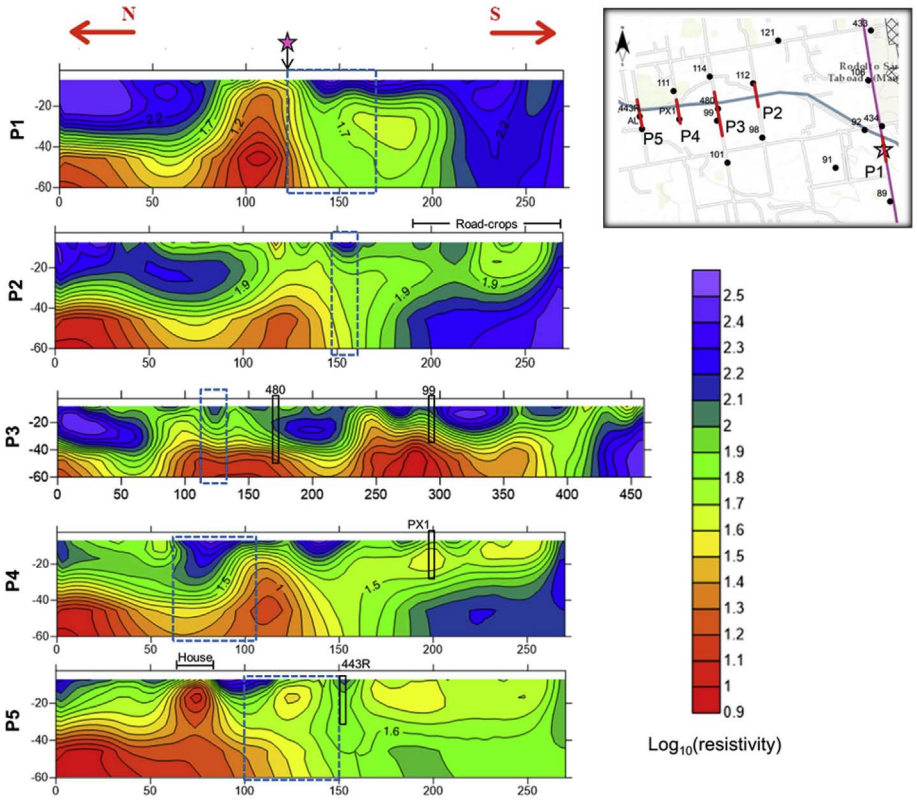

Fig. 10. 2D resistivity profiles obtained along the Las Ánimas creek. The *black rectangles* indicate the location of the wells that cross the sections and the *dash blue rectangles* the riverbed of Las Ánimas creek. The *star symbol* indicates the discharge point of RW. (For interpretation of the references to color in this figure legend, the reader is referred to the Web version of this article.)

signatures. Thus, a seasonal or multiyear timescale analysis which includes additional data (i.e. landscape component and spatial patterns) will improve the EMMA with RW as one of the end-members.

Overall, RW has similar geochemical and isotopic composition to that of groundwater with Cl^- concentrations between 1080 and 1400 mg/L (i.e. f_{SW} of 4–5%). Based on the geochemical and isotopic variations (Table 6), it is possible that RW reached the saturated zone in five wells (PX1, 211, 443R, 85, 98 and 112) during April 2016 and August 2017. This is further suggested from its location closer to the source of discharge at LAC. Nitrate and B^- concentrations in RW are almost equal in two samples (112 and 85). This leads to the previous hypothesis that the mix with RW result in effects on cation-exchange and adsorption reactions and once clay minerals reach a steady state with respect to the ions, Na^+, Br^- and B^- for example remain dissolved in groundwater.

4.4. Aquifer recharge assessment

The $\delta^{18}O_{H2O}$ and $\delta^{2}H_{H2O}$ of groundwater in Maneadero lies within the GMWL and the mixing line with seawater (Fig. 6), which denotes both the meteoric origin and the effect of seawater intrusion. However, variations in $\delta^{18}O_{H2O}$ with respect to Cl^- concentrations (Fig. 7a) reflect that leachate of evaporites and volcanic rocks is responsible for salinization besides seawater. The isotopic composition of the springs also lies within the range of the mixing line and the isotopic signature of the origin is similar to that of the Agua Caliente hot spring, which suggests the geothermal contribution.

The *d*-excess values from +0.9 to +9.7‰ (Table 1) are indicative of modern recharge. The lowest *d*-excess values (up to +3.1) are found in two samples near the coast; whereas highest values close to the LAC of +10‰ are observed in most of the wells located in the upper parts of the creeks. The *d*-excess of 10‰ is the typical average of GMWL derived from ocean moisture sources (IAEA, 2006), and result from the dominant precipitation of recharge in this area. In March 2017, during a rainfall event, the water stable isotopes in samples 89, 374 and 112 (Table 6) located along the Las Ánimas creek, were more negative and *d*-excess coincided with the LAC. Sample 112 had the most negative isotopic composition (−10.5‰ for $\delta^{18}O_{H2O}$ and −74.0‰ for $\delta^{2}H_{H2O}$). These findings for water isotopes suggest two water recharges: (1) local rain with isotopic composition of the LAC of -6.04δ for $^{18}O_{H2O}$ and −38.2 for $\delta^{2}H_{H2O}$ and (2) lateral flow from the upstream catchment with negative isotopic composition to that of sample 112.

The *d*-excess between 5 and 6‰ is similar to RW and extends through most of the central part of the aquifer and in locations nearby the Las Ánimas creek. These values, however, can be suggestive of local recharge from different isotopic compositions. When precipitation recharge is not available, it seems that groundwater is limited for local recharge, which may derive from solid waste, urban wastewater and animal waste as identified by the Cl/Br ratios salinity regimes, including RW (Fig. 5a). The contribution of these sources can be favored by the high permeability in this area, which is observed in the temporal variations of the hydrochemistry and water stable isotopes. Yet, the $\delta^{18}O_{H2O}$ did not provide information about the preferential flow path in the area. The study area is bound by the Agua Blanca fault and other tectonic faults (Arango-Galván et al., 2015) and likely crossed by minor faults in different directions that may form conduits for groundwater flow. Further, changes in flow paths can be affected by over-abstraction (Horton et al., 1999). Thus, flow paths should be studied in the region and any attempts to evaluate the hydrological balances must take into consideration the fact that an important component of the recharge may derived from the anthropogenic sources besides the natural replenishment.

4.5. Sources of nitrates in groundwater

Analysis of nitrate isotopes distinguishes NH_4^+-fertilizers, soil organic N, wastewater and manure as the main sources responsible for nitrate concentrations (Fig. 9). Natural soil organic N is reflected in the surface water at the LAC. The RW effluent has similar isotopes signatures to the effluents reported by Archana et al. (2016) derived from secondary and chemically enhanced primary treatments, and resembles the sewage component. Groundwater contamination derived from wastewater is likely due to the historical use of latrines (Daesslé et al., 2014) and to the lack of proper domestic waste disposal facilities that continues to the present day, rather than RW after treatment. High nitrate content is also found in areas where mixed crop-livestock farming occurs; making NH_4^+ fertilizers and animal waste (i.e. dung and urine) other potential sources of nitrates. However, the contribution from nitrification of NH_4^+ fertilizers seems to be negligible indicated by the measured $\delta^{15}N_{NO3}$ values which are higher compared to what would be expected with mineral fertilizers as main source. Further, nitrate isotope data are in agreement with Cl/Br ratios as indicators of impact derived from domestic wastewater and animal waste. The reason that excessive enrichment of +86‰ for $\delta^{15}N_{NO3}$ occurred at well 87 from December 2016 remains unknown.

Given the potential nitrate sources, nitrification should be taken into account. If nitrate of groundwater is generated via nitrification, a rough estimation of$\delta^{18}O_{NO3}$ can be as follows (Snider et al., 2010):

$$\delta 1^{8}O_{NO3} = 1/3\delta^{18}O_{O2} + 2/3\delta^{18}O_{H2O} \quad (7)$$

Where $\delta^{18}O_{O2}$ is the signature of dissolved oxygen which is about +23.5‰ (Kendall, 1998) and $\delta^{18}O_{H2O}$ is the measured isotope signature of water which ranges from −10.5 to −4.8‰ (only shown for March 2017, Table 6). Consequently, the expected $\delta^{18}O_{NO3}$ derived from nitrification should be in the range of +0.8 to +4.6‰, which is the case for half of the samples. However, depending on the composition of the nitrifying microbial community, an uncertainty of a few per mil may be introduced to Eq. (7) due to a kinetic isotope effect during nitrite oxidation (Buchwald and Casciotti, 2010). During nitrification, organic nitrogen is oxidized to NO_3^--N, becoming enriched in lighter isotopes and depleted in heavier isotopes relative to the substrate pool (Kendall, 1998) as observed in the temporal variations of five samples (434, 112, 120, 114 and 520R). The $\delta^{15}N_{N2O}$ and $\delta^{18}O_{N2O}$ in two samples (480 and 114) located close to each other along the Las Ánimas creek became enriched with a $\delta^{15}N/\delta^{18}O$ ratio that ranges from 1 to 2, indicating the potential occurrence of denitrification (Böttcher et al., 1990; Fukada et al., 2003).

As for RW, no sample reflected the effluent isotope nitrate composition, including sample 112 in which hydrochemical and nitrate compositions are comparable to RW. Toze et al. (2004) found that NO_3^--N in the recovery water were higher than the infiltrated RW, but always ≤6 mg/L. They attributed the increase in NO_3^--N to nitrification processes. Contrary, Schmidt et al. (2011) found that NO_3^--N < 6 mg/L in a managed infiltrating effluent decreased during passage through the first meter of subsurface soils mostly to denitrification followed by dilution at depth. These processes could explain the negligible nitrate stable isotope fingerprint from RW and, if so, it remains to be tested and determined whether these processes may occur elsewhere in the study area. Furthermore, a characterization of minerals could further elucidate these and other processes.

4.6. Electrical resistivity profiles

The interpretation of ERT profiles (Fig. 10) suggests that resistivities (log 10) > 2 (in blue) represent groundwater of lower TDS (< 1500 mg/L) and probably gravel-sand mixtures during dry conditions; whilst resistivities < 1.5 (in orange-red) probably indicate the influence of brackish water with TDS ≥5000 mg/L. As for RW, the effluent is identified in the range of 1.6–1.9 (in green). The RW plume appears to travel laterally and down gradient through the high permeable zone and is likely driven between the low and high saline water by density-differences convection. Over-pumping contributes to

seawater intrusion by upward flowing of salt-water as shown in P3 where the section crosses the location of wells 99 and 480, and also in the other sections. However, groundwater pumping may also already be moving infiltrating RW water upwards as suggested by the wells PX1 and 443R which are crossed by sections P4 and P5, and have also been identified by their chemistry as RW-influenced sites.

4.7. Conclusions and opportunities for aquifer recharge with RW

Hydrochemical and isotopic analyses show that the Maneadero aquifer is a mix of dissolved salts attributed to evaporites and volcanic rocks, anthropogenic-derived processes and seawater intrusion. Dissolution of evaporites and reverse ion exchange are the major processes influencing the groundwater chemistry. Urban solid waste, wastewater and animal waste are the main anthropogenic inputs to the aquifer. The groundwater appears to be of modern recharge, it has a meteoric origin and dilution by seawater responsible for the variations in water isotopic signatures along with a superimposed hydrothermal component in groundwater. The parameters of groundwater and RW are higher than the desired values as determined in the SPI. However, RW used for irrigation purposes is considered acceptable in the region.

The hydrochemical results suggest that the recharge with RW results in cation-exchange and adsorption reactions and once the adsorbed sites become saturated, Na^+, Br^- and B^- for example remain dissolved in groundwater. In the view of nitrates, it remains to be tested whether NO_3^--N in RW during infiltration are removed due to denitrification processes and/or to the conversion of NH_4^+ to NO_3^--N and, ultimately, if nitrates are diluted by the effluent.

Hydrogeochemical and geophysical evidence suggests that RW has probably reached wells located > 1 km downstream from the discharge spot, indicating high permeability conditions for the site. As part of a managed aquifer recharge project, the quality of RW could be eventually improved by taking advantage of contaminant attenuation processes. In this matter, the results from this study show that the capacity of soil to adsorb PO_4^{3-}P and K^+ is reached. However, the long-term recharge of RW with high levels of these elements could lead to a steady state with respect to these elements and be reflected in the composition of groundwater. It is essential to monitor these and other organic pollutants such as emerging medical residues and pesticides, to predict groundwater contamination. Because the aquifer was already contaminated by seawater intrusion and nitrates previous to the discharge, it is also important to distinguish sources for these and other contaminants from the RW effluent source.

Considering the favorable conditions for an aquifer recharge in the region, the recharge with RW can be implemented by an appropriate planning, water quality control, precautions and an additional treatment; e.g. membrane techniques for TDS and boron removal. Pilot recharge tests must be conducted, which include research of residence times for the infiltrated RW, the extent of mixing with the groundwater, time scales and preferential flow paths and should be thoroughly studied in the area. In addition, regulations should be undertaken to avoid the leach of contaminants derived from urban solid waste and wastewater and animal waste. These factors must be considered for aquifer recharge locations, as well as the risks of fertilizers and dissolved salts from the irrigated areas to reach the saturated zone.

Acknowledgements

This work received funding from UABC through the 18th call for research proposals (grant 632). C. Gilabert and S. Salgado were supported by the Mexican Council for Science and Technology (CONACYT) through PhD grants 414727 and 279742, and an international exchange fellowship at UFZ-Helmholtz for C. Gilabert, as well as a sabbatical fellowship (266073) to L.W. Daesslé at CICESE. We acknowledge CONACYT and SENER for their support through the CeMIE-Geo project (grant 207032) to T. Kretzschmar, and are especially grateful to Fernando Herrera for the resistivity measurements, Ana Karina Espinosa for doing part of the anion analyses and Petra Seibel for help with the stable isotopes. Also to Alejandro Guzmán, manager of the Maneadero aquifer technical council for his valuable support and the two anonymous reviewers for their suggestions and critical comments. This paper is dedicated to our late colleague Eduardo Ortiz Campos† for his friendship and ever so professional support in the field and laboratory at UABC, during this and many other projects.

References

Alcalá, F.J., Custodio, E., 2008. Using the Cl/Br ratio as a tracer to identify the origin of salinity in aquifers in Spain and Portugal. J. Hydrol 359 (1–2), 189–207. https://doi.org/10.1016/j.jhydrol.2008.06.028.

Alvaréz, M.J., 1949. Unidades tectónicas de la República Mexicana (Tectonic units of the Mexican Republic). Bol. Soc. Geológica Mexicana 14, 1–22.

Appelo, C.A.J., Postma, D., 2005. Geochemistry, Groundwater, and Pollution, second ed. CRC Press.

AQUAVEO, 2016. Arc Hydro Groundwater Software. https://www.aquaveo.com/ (AccessedJanuary2017).

Arango-Gavlán, C., Prol-Ledesma, R.M., Flores-Márquez, E.L., Canet, C., Estrada, R.E.V., 2011. Shallow submarine and subaerial, low-enthalpy hydrothermal manifestations in Punta Banda, Baja California, Mexico: geophysical and geochemical characterization. Geotherrmics 40 (2), 102–111. https://doi.org/10.1016/j.geothermics.2011.03.002.

Arango-Gavlán, C., Prol-Ledesma, R.M., Torres-Vera, M.A., 2015. Geothermal prospects in the Baja California Peninsula. Geotherrmics 55, 39–57. https://doi.org/10.1016/j.geothermics.2015.01.005.

Archana, A., Li, L., Shuh-Ji, K., Thibodeau, B., Baker, D.M., 2016. Variations in nitrate isotopes composition of wastewater effluents by treatment type in Hong Kong. Mar. Pollut. Bull. 111 (1–2), 143–152. https://doi.org/10.1016/j.marpolbul.2016.07.019.

Argamasilla, M., Barberá, J.A., Andreo, B., 2017. Factors controlling groundwater salinization and hydrogeochemical processes in coastal aquifers from southern Spain. Sci. Total Environ. 580, 50–68. https://doi.org/10.1016/j.scitotenv.2016.11.173.

Asano, T., Cotruvo, J.A., 2004. Groundwater recharge with reclaimed municipal wastewater: health and regulatory considerations. Water Res. 38 (8), 1941–1951. https://doi.org/10.1016/j.watres.2004.01.023.

Barthold, F.K., Tyralla, C., Schneider, K., Vaché, K.B., Hans-Georg, F., Breuer, L., 2011. How many tracers do we need for end member mixing analysis (EMMA)? A sensitivity analysis. Water Resour. Res. 47 (8), 1–14. https://doi.org/10.1029/2011WR010604.

Bekele, E., Patterson, B., Toze, S., Furness, A., Higginson, S., Schackleton, M., 2014. Aquifer residence times for recycled water estimated using chemical tracers and the propagation of temperature signals at a managed aquifer recharge site in Australia. Hydrogeol. J. 22 (6), 1383–1401. https://doi.org/10.1007/s10040-014-1142-0.

Bekele, E., Toze, S., Patterson, B., Higginson, S., 2011. Managed aquifer recharge of treated wastewater: water quality changes resulting from infiltration through the vadose zone. Water Res. 45 (17), 5764–5772. https://doi.org/10.1016/j.watres.2011.08.058.

Bouchaou, L., Michelot, J.L., Vengosh, A., Hsissou, Y., Qurtobi, M., Gaye, C.B., Bullen, T.D., Zuppi, G.M., 2008. Application of multiple isotopic and geochemical tracers for investigation of recharge, salinization, and residence time of water in the Souss-Massa aquifer, southwest of Morocco. J. Hydrol 352 (3–4), 267–287. https://doi.org/10.1016/j.jhydrol.2008.01.022.

Bouzourra, H., Bouhlila, R., Elango, L., Slama, F., Ouslati, N., 2015. Characterization of mechanisms and processes of groundwater salinization in irrigated coastal area using statistics, GIS, and hydrogeochemical investigations. Environ. Sci. Pollut. Res. 22 (4), 2643–2660. https://doi.org/10.1007/s11356-014-3428-0.

Böttcher, J.K., Strebe, O., Voerkelius, S., Schmidt, H.L., 1990. Using isotope fractionation of nitrate-nitrogen and nitrate-oxygen for evaluation of microbial denitrification in a sandy aquifer. J. Hydrol 114 (3–4), 413–424. https://doi.org/10.1016/0022-1694(90)90068-9.

Buchwald, C., Casciotti, K.L., 2010. Oxygen isotopic fractionation and exchange during bacterial nitrite oxidation. Limnol. Oceanogr. 55 (3), 1064–1074. https://doi.org/10.4319/lo.2010.55.3.1064.

Casciotti, K.L., Sigman, D.M., Hastings, M.G., Böhlke, J.K., Hilkert, A., 2002. Measurement of the oxygen isotopic composition of nitrate in seawater and freshwater using the denitrifier method. Anal. Chem. 74 (19), 4905–4912. https://doi.org/10.1021/ac020113w.

Chen, J., Tang, C., Yu, J., 2006. Use of Use of ^{18}O, ^{2}H and ^{15}N to identify nitrate contamination of groundwater in a wastewater irrigated field near the city of Shijiazhuang, China. J. Hydrol 326 (1), 367–378. https://doi.org/10.1016/j.jhydrol.2005.11.007.

Christophersen, N., Hooper, R.P., 1992. Multivariate analysis of stream water chemical data: the use of principal component analysis for the end-member mixing problem. Water Resour. Res. 28 (1), 99–107. https://doi.org/10.1029/91WR02518.

Cloutier, V., Lefebvre, R., Therrien, R., Savard, M.M., 2008. Multivariate statistical analysis of geochemical data as indicative of the hydrogeochemical evolution of groundwater in a sedimentary rock aquifer system. J. Hydrol. (Wellingt. North) 353 (3–4), 294–313. https://doi.org/10.1016/j.jhydrol.2008.02.015.

CONAGUA, 1999. Estudio de simulación hidrodinámica del acuífero de Maneadero, B.C. (Hydrodinamic simulation model of the Maneadero aquifer, Baja California).

Subdirección Técnica-Gerencia aguas subterráneas.
Craig, H., 1961. Isotopic variations in meteoric water. Science 133 (3465), 1702–1703. https://doi.org/10.1126/science.133.3465.1702.
Custodio, E., Llamas, M.R., 1996. Hidrologíasubterránea (Groundwater Hydrology), second ed. Omega.
Daesslé, L.W., Pérez-Flores, M.A., Serrrano-Ortiz, J., Mendoza-Espinosa, L., Manjarrez-Masuda, E., Lugo-Ibarra, K.C., Gómez-Treviño, E., 2014. A geochemical and 3D-geometry geophysical to assess artificial groundwater recharge potential in the Pacific coast of Baja California, Mexico. Environ. Earth Sci. 71 (8), 3477–3490. https://doi.org/10.1007/s12665-013-2737-9.
Daesslé, L.W., Ruiz-Montoya, I., Tobschall, H.J., Chandrajith, R., Camacho-Ibar, V.F., Mendoza-Espinosa, L.G., Quintanilla-Montoya, A.L., Lugo-Ibarra, K.C., 2009. Fluoride, nitrate and water hardness in groundwater supplied to the rural communities of Ensenada County, Baja California. Mexico.Environ. Geol. 58 (2), 419–429. https://doi.org/10.1007/s00254-008-1512-9.
Daesslé, L.W., Sánchez, E.C., Camacho-Ibar, V.F., Mendoza-Espinosa, L.G., Carriquiry, J.D., Macias, V.A., Castro, P.G., 2005. Geochemical evolution of groundwater in the Maneadero coastal aquifer during a dry year in Baja California. Mexico.Hydrogeol.J 13 (4), 584–595. https://doi.org/10.1007/s10040-004-0353-1.
Daesslé, L.W., Orozco, A., Struck, U., Camacho-Ibar, V.F., van Geldern, R., Santamaría-del-Angel, E., Barth, J.A.C., 2017. Sources and sinks of nutrients and organic carbon during the 2014 pulse flow of the Colorado River into Mexico. Ecol. Eng. 106 (Part B), 799–808. https://doi.org/10.1016/j.ecoleng.2016.02.018.
Daesslé, L.W., van Geldern, R., Orozco-Durán, A., Barth, J.A.C., 2016. The 2014 water release into the arid Colorado River delta and associated water losses by evaporation. Sci. Total Environ. 542 (Part A), 586–590. https://doi.org/10.1016/j.scitotenv.2015.09.157.
Dansgaard, W., 1964. Stable isotopes in precipitation. Tellus 16 (4), 436–468. https://doi.org/10.1111/j.2153-3490.1964.tb00181.x.
Davis, N., Whittemore, D.O., Fabryka-Martin, J., 1998. Uses of chloride/bromide ratios in studies of potable water. Groundw 36 (2), 338–350. https://doi.org/10.1111/j.1745-6584.1998.tb01099.x.
De Bustamante, I., Cabrera, M.C., Candela, L., Lilio, J., Palacios, M.P., 2010. La reutilización de aguas regeneradas en España: ejemplos de aplicación en el marco del proyecto CONSOLIDER-TRAGUA (Treated urban wastewater reuse in Spain: the CONSOLIDER-TRAGUA project case study examples). Agua-LAC 2 (1), 1–17.
De Montety, V., Radakovitch, O., Vallet-Coulomb, C., Blavoux, B., Hermitte, D., Valles, V., 2008. Origin of groundwater salinity and hydrochemical processes in a confined coastal aquifer: case of Rhône delta (Southern France). Appl. Geochem. 23 (8), 2337–2349. https://doi.org/10.1016/j.apgeochem.2008.03.011.
De Vries, J.J., Simmers, I., 2002. Groundwater recharge: an overview and processes and challenges. Hydrogeol. J. For 10 (1), 5–17. https://doi.org/10.1007/s10040-001-0171-7.
Dimitrov, D.M., 2012. Statistical Methods for Validation Assessment Scale Data in Counseling and Related Field. American Counseling Association.
Dixon, W., Chiswell, B., 1992. The use of hydrochemical sections to identify recharge areas and saline intrusions in alluvial aquifers, southeast Queensland, Australia. J. Hydrol 135 (1–4), 259–274. https://doi.org/10.1016/0022-1694(92)90091-9.
DOF, 2001. Norma Oficial Mexicana NOM-127-SSA-1994, salud ambiental, agua para uso y consume humano-límites permisibles de calidad y tratamientos a que se debe someterse el agua para su potabilización (Mexican official norm NOM-127-SSA-1994, environmental health, permissible quality limits of water for use and human consumption and treatments for potabilization). Secretaría de Gobernación, Mexico.
DOF, 2015. ACUERDO por el que se actualiza la disponibilidad media anual de agua subterránea de los 653 acuíferos de los Estados Unidos Mexicanos, mismos que forman parte de las regiones hidrológico-administrativas que se indican (AGREEMENT that updates the average annual groundwater availability of 653 aquifers, which are part of the hydrological-administrative regions). Secretaría de Gobernación, Mexico.
Donohue, S., McCarthhy, V., Rafferty, P., Orr, A., Flynn, R., 2015. Geophysical and hydrogeological characterization of the impacts of on-site wastewater treatment discharge to groundwater in a poorly productive bedrock aquifer. Sci. Total Environ. 523 (1), 109–119. https://doi.org/10.1016/j.scitotenv.2015.03.117.
ERSI, 2017. Arc GIS Map (Version 10.2). http://www.ersi.com/en-us/home (Accessed March 2017).
Foster, S., Garduño, H., Tuinhof, A., Kemper, K., Nanni, M., 2003. Recarga del agua subterránea con aguas residuales urbanas: evaluación y manejo de los riesgos y beneficios (Urban wastewater as groundwater recharge: evaluating and managing the risks and benefits). World Bank, , Washington, DC GW Mate briefing note series no. 12. http://documents.worldbank.org/curated/en/378851468328599437/Recarga-del-agua-subterranea-con-aguas-residuales-urbanas-evaluacion-y-manejo-de-los-riegos-y-beneficios (Accessed April 2017).
Foued, E.A., Semia, C., Amel, J., Malika, T.A., 2011. Impact of treated wastewater reuse on agriculture and aquifer recharge in a coastal area: Korba case study. Water Resour. Manag. 25 (9), 2251–2265. https://doi.org/10.1007/s11269-011-9805-2.
Freeze, R.A., Cherry, J.A., 1979. Groundwater. Prentice Hall, Englewood Cliffs.
Fukada, T., Hiscock, K.M., Dennis, P.F., Grischek, T., 2003. A dual isotope approach to identify denitrification in groundwater at a river-bank infiltration site. Water Res. 37 (13), 3070–3078. https://doi.org/10.1016/S0043-1354(03) 00176–3.
Gautam, K.S., Maharana, C., Sharma, D., Singh, A.K., Tripathi, J.K., Singh, S.K., 2015. Evaluation of groundwater quality in the Chotanagpur plateau region of the Subarnarekha river basin, Jharkand State, India. Sustain. Water Qual. Ecol 6, 57–74. https://doi.org/10.1016/j.swaqe.2015.06.001.
Goebel, M., Pidlisecky, A., Knight, R., 2017. Resistivity imaging reveals complex pattern of saltwater intrusion along Monterey coast. J. Hydrol 551, 746–755. https://doi.org/10.1016/j.jhydrol.2017.02.037.
Hair, J.F., Black, W.C., Babin, B.J., Anderson, R.E., 2010. Multivariate Data Analysis, seventh ed. Prentice Hall.
Han, D., Kohfahl, C., Song, X., Xiao, G., Yang, J., 2011. Geochemical and isotopic evidence for paleo-seawater intrusion into the south coast aquifer of Laizhou Bay, China. Appl. Geochem. 26 (5), 863–883. https://doi.org/10.1016/j.apgeochem.2011.02.007.
Hounslow, A., 1995. Water Quality Data: Analysis and Interpretation. CRC Press.
Horton, T.W., Chamberlain, C.P., Fantle, M., Blum, J.D., 1999. Chemical weathering and lithologic controls of water chemistry in a high-elevation river system: Clark's Fork of the Yellowstone River, Wyoming and Montana. Water Resour. Res. 35 (5), 1643–1655. https://doi.org/10.1029/1998WR900103.
IAEA, 2006. Global Network of Isotopes in Precipitation. International Atomic Energy Agency. Vienna.
Isaaks, E., Srivastava, R.M., 1989. An Introduction to Applied Geostatistics. Oxford University Press.
James, A.L., Roulet, N.T., 2006. Investigating the applicability of end-member mixing analysis (EMMA) across scale: a study of eight small, nested catchments in a temperate forested watershed. Water Resour. Res. 42 (8), 1–17. https://doi.org/10.1029/2005WR004419.
Jeen, S.W., Kim, J.M., Ko, K.S., Yum, B., Chang, H.W., 2001. Hydrogeochemical characteristics of groundwater in a mid-western coastal aquifer system. Korea, Geosci. J. 5 (4), 339–348. https://doi.org/doi.org/10.1007/BF02912705.
Kabata-Pendias, A., Pendias, H., 2001. Trace Element in Soils and Plants, thirdedn. CRC Press.
Kaiser, H.F., 1960. The application of electronic computers to factor analysis. Educ. Psychol. Meas. 20 (1), 141–151. https://doi.org/10.1177/001316446002000116.
Kanarek, A., Michail, M., 1996. Groundwater recharge with municipal effluent: Dan Region reclamation project. Israel.Water. Sci. Technol 34 (11), 227–233. https://doi.org/10.1016/S0273-1223(96)00842-6.
Kendall, C., 1998. Tracing nitrogen sources and cycling in catchments. In: Kendall, McDonnell, J.J. (Eds.), Isotope Tracers in Catchment Hydrology. Elseiver Science, pp. 519–576.
Kendall, C., Elliott, E.M., Scott, D.W., 2007. Tracing anthropogenic inputs of nitrogen to ecosystems. In: Michener, R., Lajtha, K. (Eds.), Stable Isotopes in Ecology and Environmental Science, secondedn. Blackwell Publishing, Oxford, pp. 375–449. https://doi.org/10.1002/9780470691854.ch12.
Kikkawa, K., Shiga, S., 1966. Relation between halogen contents of hot spring water. Special Contrib. Geophys.Inst 6, 173–185.
Kitanidias, P.K., 1997. Introduction to Geostatistics: Applications in Hydrogeology. Cambridge University Press.
Kloppmann, W., Chikurel, H., Picot, G., Guttman, J., Pettenati, M., Ahorani, A., Guerrot, C., Millot, R., Gaus, I., Wintgens, T., 2009. B and Li isotopes as intrinsic tracers for injection tests in aquifer storage and recovery systems. Appl. Geochem. 24 (7), 1214–1223. https://doi.org/10.1016/j.apgeochem.2009.03.006.
Kummar, M., Ramanathan, A., Keshari, A.K., 2009. Understanding the extent of interactions between groundwater and surface water through major ion chemistry and multivariate statistical techniques. Hydrol. Process. 23, 297–310. https://doi.org/10.1002/hyp.7149.
Laboratoire d`Hydrogéologie d`Avignon, 2017. Diagrammes Software (Version 6.5). http://www.lha.univ-avignon.fr/LHA-Logiciels.htm.
Ledesma-Ruiz, R., Pastén-Zapata, E., Parra, R., Harter, T., Mahlknecht, J., 2015. Investigation of the geochemical evolution of groundwater under agricultural land: a case in northeastern Mexico. J. Hydrol 521, 410–423. https://doi.org/10.1016/j.jhydrol.2014.12.026.
Machiwal, D., Madan, K.J., 2015. Identifying sources of groundwater contamination in a hard-rock aquifer system using multivariate statistical analysis and GIS-based geostatistical modeling techniques. J. Hydrol 4 (A), 80–110. https://doi.org/10.1016/j.ejrh.2014.11.005.
Madioune, H.D., Faye, S., Orban, P., Brouyère, S., Dassargues, A., Mudry, J., Stumpp, C., Malosyewski, P., 2014. Application of isotopic tracers as a tools for understanding hydrodynamic behavior of the highly exploited Diass aquifer system (Senegal). J. Hydrol 511, 443–459. https://doi.org/10.1016/j.jhydrol.2014.01.037.
Manno, E., Vassallo, M., Varrica, D., Dongarrà, G., Hauser, S., 2006. Hydrogeochemistry and water balance in the coastal wetland: area of “Biviere di Gela”, Sicily, Italy. Water Air Soil Pollut. 178 (1–4), 179–193. https://doi.org/10.1007/s11270-006-9189-8.
Martínez, D.E., Bocanegra, E.M., 2002. Hydrogeochemistry and cation-exchange processes in the coastal aquifer of Mar Del Plata. Argentina.Hydrogeol. J. 10 (3), 393–408. https://doi.org/10.1007/s10040-002-0195-7.
Massmann, G., Knappe, A., Richter, D., Pekdeger, A., 2004. Investigating the influence of treated sewage on groundwater and surface water using wastewater indicators in Berlin, Germany. ActaHydrochem.Hydrobiol 32 (4–5), 336–350. https://doi.org/10.1002/aheh.200400543.
McArthur, J.M., Sikdar, P.K., Hoque, M.A., Ghosal, U., 2012. Waste-water impacts on groundwater: Cl/Br ratios and implications for arsenic pollution of groundwater in the Bengal Basin and Red River Basin. Viethnam.Sci. Total Environ 437, 390–402. https://doi.org/10.1016/j.scitotenv.2012.07.068.
Meybeck, M., 1987. Global chemical weathering of surficial rock estimated from river dissolved loads. Am. J. Sci. J 287 (5), 401–428. https://doi.org/10.2475/ajs.287.5.401.
Missimer, T.M., Drewes, J.E., Amy, G., Maliva, R.G., Stephanie, K., 2012. Restoration of wadi aquifers by artificial recharge with treated wastewater. Groundw 50 (4), 514–527. https://doi.org/10.1111/j.1745-6584.2012.00941.x.
Murray, R., 2008. Artificial Recharge: the Intentional Banking and Treating of Water in Aquifers. http://www.artificialrecharge.co.za/coursenotes/lecturenotes.pdf (Accessed November 2017).

Najib, S., Fadili, A., Mehdi, K., Riss, J., Makan, A., Guessir, H., 2016. Salinization process and coastal groundwater quality in Chaouia, Morocco. J. Afr. Earth Sci. 115, 17–31. https://doi.org/10.1016/j.jafrearsci.2015.12.010.
Okiongbo, K.S., Douglas, R.K., 2015. Evaluation of major factors influencing the geochemistry of groundwater using graphical and multivariate statistical methods in Yenagoa city. Southern Nigeria.Appl. Water Sci. 5 (1), 27–37. https://doi.org/10.1007/s13201-014-0166-x.
Orozco-Durán, A., Daesslé, L.W., Camacho-Ibar, V.F., Ortiz-Campos, E., Barth, J.A.C., 2015. Turnover and release of P-, N-, Si-nutrients in the Mexicali Valley (Mexico): interactions between the lower Colorado River and adjacent ground- and surface water systems. Sci. Total Environ. 15 (512–513), 185–193. https://doi.org/10.1016/j.scitotenv.2015.01.016.
Pakhurst, D.L., Appelo, C.A.J., 1999. User's guide to PHREEQC (version 2)-A computer program for speciation, reaction-path, ID-transport, and inverse geochemical calculations. Water Resour. Inv. Rep 99–4259.
Panno, S.V., Hackley, K.C., Hwang, H.H., Greenberg, S.E., Krapac, I.G., Landsberger, S., O´Kelly, D.J., 2006. Characterization and identification of Na-Cl sources in groundwater. Groundw 44 (2), 176–187. https://doi.org/10.1111/j.1745-6584.2005.00127.x.
Pérez-Flores, M.A., Méndez-Delgado, S., Gómez-Treviño, E., 2001. Imaging of low-frequency and DC electromagnetic fields using a simple linear approximation. Gephys 66 (4), 1067–1081. https://doi.org/10.1190/1.1487054.
Phillips, D.L., Gregg, J.W., 2003. Source partitioning using stable isotopes: coping with too many sources. Oecologia (Berl.) 136 (2), 261–269. https://doi.org/10.1007/s00442-003-1218-3.
Piper, A.M., 1944. A graphical procedure in the geochemical interpretation of water analysis. Eos, Trans. Am. Geophys. Union 25 (6), 914–923. https://doi.org/10.1029/TR025i006p00914.
Richter, C., Kreitler, C., 1993. Geochemical Techniques for Identifying Sources of Groundwater Salinization. CRC Press.
Rueedi, J., Cronin, A.A., Morris, B.L., 2009. Estimation of sewer leakage to urban groundwater using depth-specific hydrochemistry. Water Environ. J. 23 (2), 134–144. https://doi.org/10.1111/j.1747-6593.2008.00119.x.
Sappa, G., Ergul, S., Ferranti, F., Sweya, L.N., Luciani, G., 2015. Effects of seasonal change and seawater intrusion on water quality for drinking and irrigation purposes, in coastal aquifers of Dar es Salaam, Tanzania. J. Afr. Earth Sci. 105, 64–84. https://doi.org/10.1016/j.jafrearsci.2015.02.007.
Schilperoort, R.P.S., Meijer, H.A.J., Flamink, C.M.L., Clemens, F.H.L.R., 2007. Changes in isotope ratios during domestic wastewater production. Water Sci. Techol 55 (4), 93–101. https://doi.org/10.2166/wst.2007.099.
Schmidt, C.M., Fisher, A.T., Racz, A., Wheat, C.G., Los Huertos, M., Lockwood, B., 2011. Rapid nutrient load reduction during infiltration of managed aquifer recharge in an agricultural groundwater basin: Parajo Valley, California. Hydrol. Proccess 26 (15), 2235–2247. https://doi.org/10.1002/hyp.8320.
Sigman, D.M., Casciotti, K.L., Andreani, M., Barford, C., Galanter, M., Böhlke, J.K., 2001. A bacterial method for the nitrogen isotopic analysis of nitrate in seawater and freshwater. Anal. Chem. 73 (17), 4145–4153. https://doi.org/10.1021/ac010088e.
Sikora, L.G., Bent, M.G., Corey, R.B., Keeney, D.R., 1976. Septic nitrogen and phosphorus removal test system. Groundw 14 (5), 309–314. https://doi.org/10.1111/j.1745-6584.1976.tb03120.x.
Silva, S.R., Ging, P.B., Lee, R.W., Ebbert, J.C., Tesoriero, A.J., Inkpen, E.L., 2002. Forensic applications of nitrogen and oxygen isotopes in tracing nitrate sources in urban environments. Environ. Forensics 3 (2), 125–130. https://doi.org/10.1006/enfo.2002.0086.
Singh, K.P., Malik, A., Mohan, D., Sinha, S., 2004. Multivariate statistical techniques for the evaluation of spatial and temporal variations in water quality of Gomti River (India)-a case study. Water Res. 38 (18), 3980–3992. https://doi.org/10.1016/j.watres.2004.06.011.
Singh, K.P., Srivastava, P.K., Singh, D., Han, D., Gautam, S.K., Pandey, A.C., 2014. Modeling groundwater quality over humid subtropical region using numerical indices, earth observation datasets, and X-ray diffraction technique: a case study of Allahabad district, India. Environ. Geochem. Health 37 (1), 157–180. https://doi.org/10.1007/s10653-014-9638-z.
Spiteri, C., Van Cappellen, P., Regnier, P., Meile, C., Slomp, C.P., 2008. Phosphate mobilization in coastal aquifers due to seawater intrusion: a model assessment. In: GQ07 IAHS Red Book, pp. 396–403.
Snider, D.M., Spoelstra, J., Schiff, S.L., Venkiteswaran, J.J., 2010. Stable oxygen isotope ratios of nitrate produced from nitrification: 18O-Labeled water incubations of agricultural and temperate forest soils. Environ. Sci. Technol. 44 (14), 5358–5364. https://doi.org/10.1021/es1002567.
State of California, 2000. Code of Regulation Title 22, Division 4, Chapter 3:Water Recycling Criteria. California, USA.
Statsoft, Inc, 2013. STATISTICA Data Analysis Software System (Version 12). http://statistica.io/ (Accessed on January 2017).
Stiff Jr., H.A., 1951. The interpretation of chemical water analysis by means of patterns. J. Petrol. Technol. 3 (10), 100–108. https://doi.org/10.2118/951376-G.
Stumpp, C., Ekdal, A., Gönenc, E., Maloszewski, P., 2014. Hydrological dynamics of water sources in a Mediterranean lagoon. Hydrol. Earth Sci. 18, 4825–4837. http://dx.doi.org/10.5194/hess-18-4825-2014. https://doi.org/.
Sugiura, T., 1968. Bromine to chlorine ratios in igneous rocks. Bull. Chem. Soc. Jpn. 41 (5), 1133–1139. https://doi.org/10.1246/bcsj.41.1133.
Taheri, M., Gharaie, M.H.M., Mehrzad, J., Afshari, R., Datta, S., 2017. Hydrogeochemical and isotopic evaluation of arsenic contaminated waters in an argillic alteration zone. J. Geochem. Explor. 175, 1–10. https://doi.org/10.1016/j.gexplo.2016.12.005.
Tellam, J.H., Llyod, J.W., 1986. Problems in the recognition of seawater intrusion by chemical means: an example of apparent chemical equivalence. G.J. Eng. Geol. Hydrogeol 19 (4), 389–398. https://doi.org/10.1144/GSL.QJEG.1986.019.04.05.
Todd, D.K., 1980. Groundwater Hydrology, second ed. Wiley.
Toze, S., Hanna, J., Smith, T., Edmonds, L., McCrow, A., 2004. Determination of water quality improvements due to the artificial recharge of treated effluent. In: In: Steenvoorden, J., Endreny, T. (Eds.), International Symposium on Wastewater Re-use and Groundwater Quality, vol. 28. Int. Assoc. Hydrological Sciences, Wallingford, UK, pp. 53–60.
USEPA, 1986. Quality criteria for water. U.S. Environ. Protection Agency Rep 86 (1) EPA 440/5.
USGS, 1999. The Quality of Our Nation's Waters, Nutrients and Pesticides. https://pubs.usgs.gov/circ/1999/1225/report.pdf (Accessed August 2017).
Vandenbohede, A., Van Houtte, E., Lebbe, L., 2009. Water quality changes in the dunes of the western Belgian coastal plain due to artificial recharge of tertiary treated wastewater. Appl. Geochem. 24 (3), 371–382. https://doi.org/10.1016/j.apgeochem.2008.11.023.
Venegas, R., 2007. Aptitud territorial: una aproximación hacia la planeación y ordenamiento de lterritorio (Territorial aptitude: an approach towards the planning and ordering of the territory). UABC.
Vengosh, A., 2003. Salinization and saline environments. Treatise on Geochem 9, 1–35. https://doi.org/10.1016/B0-08-043751-6/09051-4.
Vengosh, A., 2014. Salinization and saline environments. Treatise on Geochem 11, 325–378. https://doi.org/10.1016/B978-0-08-095975-7.00909-8.
Vengosh, A., Benzvi, A., 1994. Formation of a salt plume in the coastal-plain aquifer of Israel- the Beer-Toviyya Region. J. Hydrol 160 (1–4), 21–52. https://doi.org/10.1016/0022-1694(94) 90032–90039.
Vengosh, A., Gill, J., Davisson, M.L., Hudson, G.B., 2002. A multi-isotope (B, Sr, O, H, and C) and age dating (^{3}H–^{3}He and ^{14}C) study of groundwater from Salinas Valley, California: hydrochemistry, dynamics, and contamination processes. Water Resour. Res. 38 (1), 9.1–9.17. https://doi.org/10.1029/2001WR000517.
Vengosh, A., Keren, R., 1996. Chemical modifications of groundwater contaminated by recharge of treated sewage effluent. J. Contam. Hydrol. 23 (4), 347–360. https://doi.org/10.1016/0169-7722(96)00019-8.
Vengosh, A., Pankratov, I., 1998. Chloride/bromide and chloride/fluoride ratios of domestic sewage effluents and associated contaminated groundwater. Groundw 3 (5), 815–824. https://doi.org/10.1111/j.1745-6584.1998.tb02200.x.
Vidal-Lorandi, V.M.V., Vidal-Lorandi, F.V., 2003. Geothermometry of the coastal submarine hydrothermal system off Punta Banda, Baja California. In: Soto, L.A. (Ed.), Agustín Ayala-Castañares: universitario, impulsor de la investigación científica (Agustín Ayala-Castañares: university, promoter of scientific research). UNAM, Mexico, pp. 111–121.
Voudouris, K., 2011. Artificial recharge via borehole using treated wastewater: possibilities and prospects. Water 3 (4), 964–975. https://doi.org/10.3390/w3040964.
Voutsis, N., Kelepertrtzis, E., Tziritis, E., Kelepertsis, A., 2015. Assessing the hydrogeochemistry of groundwater in ophiolite areas of Euboea Island, Greece, using multivariate statistical methods. J. Geochem. Explor. 159, 79–92. https://doi.org/10.1016/j.gexplo.2015.08.007.
Wang, S., Tang, C., Song, X., Wang, Q., Zhang, Y., Yuan, R., 2014. The impacts of a linear wastewater reservoir on groundwater recharge and geochemical evolution in a semi-arid area of the Lake Baiyangdian watershed, North China Plain. Sci. Total Environ. 482–483 (1), 325–335. https://doi.org/10.1016/j.scitotenv.2014.02.130.
Ward, J.H., 1963. Hierarchical grouping to optimize an objective function. J. Am. Stat. Assoc. 58 (301), 236–244. https://doi.org/10.1080/01621459.1963.10500845.
WHO, 2011. Guidelines for Drinking-water Quality, fourth ed. . http://www.who.int/water_sanitation_health/publications/2011/dwq_guidelines/en/ (Accessed March 2017).
Wolfsberg, M., Van Kook, W.A., Paneth, P., Rebelo, L.P.N., 2009. Isotope Effects: in the Chemical, Geological, and Bio Sciences. Springer Science & Business Media.
Xue, D., Botte, J., De Baets, B., Accoe, F., Nestler, A., Taylor, P., Van Cleemput, O., Berglund, M., Boeckx, P., 2009. Present limitations and future prospects of stable isotope methods for nitrate source identification in surface-an groundwater. Water Res. 43 (5), 1159–1170. https://doi.org/10.1016/j.watres.2008.12.048.
Yidana, S.M., Banoen-Yakubo, B., Akabyaa, T.M., 2010. Analysis of groundwater quality using multivariate and spatial analyses in the Keta basin, Ghana. J. Afr. Earth Sci. 58, 220–234. https://doi.org/10.1016/j.jafrearsci.2010.03.003.